Agricultural and Forest Meteorology 367 (2025) 110486

Contents lists available at ScienceDirect

Agricultural and Forest Meteorology

journal homepage: www.elsevier.com/locate/agrformet

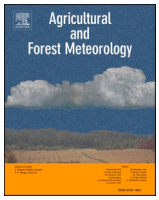

Modeling carbon and water fluxes in agro-pastoral systems under contrasting climates and different management practices

L. Leolini [a], S. Costafreda-Aumedes [b,*], L. Brilli [b], M. Galvagno [c], M. Bindi [a], G. Argenti [a], D. Cammarano [d], E. Bellini [a], C. Dibari [a], G. Wohlfahrt [e], I. Feigenwinter [f], A. Dal Prà [b], D. Dalmonech [g,h], A. Collalti [g,h], E. Cremonese [i], G. Filippa [c], N. Staglianò [a], M. Moriondo [a,b]

[a] Department of Agriculture, Food, Environment and Forestry (DAGRI), University of Florence, Piazzale delle Cascine 18, 50144 Florence, Italy
[b] National Research Council of Italy, Institute of BioEconomy (CNR-IBE), Via Madonna del Piano 10, 50019 Sesto Fiorentino, Italy
[c] Environmental Protection Agency of Aosta Valley, Climate Change Dept, ARPA VdA, Loc. La Maladière 48, 11020 Saint Christophe, Italy
[d] Department of Agroecology, iClimate, CBIO, Aarhus University, iClimate, Centre for Circular Bioeconomy (CBIO), Blichers Allé 20, DK-8830 Tjele, Denmark
[e] Universität Innsbruck, Institut für Ökologie, Sternwartestrasse 15, 6020 Innsbruck, Austria
[f] Department of Environmental Systems Science, Institute of Agricultural Sciences, ETH Zurich, Universitätstrasse 2, 8092 Zurich, Switzerland
[g] Forest Modelling Laboratory, Institute for Agriculture and Forestry Systems in the Mediterranean, National Research Council of Italy (CNR-ISAFOM), 06128 Perugia, Italy
[h] National Biodiversity Future Center (NBFC), 90133 Palermo, Italy
[i] CIMA Research Foundation, Via A. Magliotto, 2 17100 Savona, Italy

ARTICLE INFO

Keywords:
Above-ground biomass
Biogeochemical cycles
Crop models
Grasslands

ABSTRACT

Grasslands are worldwide spread ecosystems involved in the provision of multiple functional services, including biomass production and carbon storage. However, the increasingly adverse climate and non-optimised farm management are threatening these ecosystems. In this study, the original semi-mechanistic remotely sensed-driven VISTOCK model, which simulates grass growth as limited by thermal and water stress, was modified and integrated with the RothC model to simulate the ecosystem fluxes. The new model (GRASSVISTOCK) showed satisfactory performance in simulating above-ground biomass (AGB) in dry matter (d.m.) and fractional transpirable soil water (FTSW) along Alps (AGB, RMSE = 85.39 g d.m. m^{-2}; FTSW, RMSE = 0.21) and Mediterranean (AGB, RMSE = 136.84 g d.m. m^{-2}; FTSW, RMSE = 0.13) grasslands. Also, GRASSVISTOCK was able to simulate the net ecosystem exchange (NEE - RMSE = 0.03 Mg C ha^{-1}), the gross primary production (RMSE = 0.04 Mg C ha^{-1}), the ecosystem respiration (RMSE = 0.04 Mg C ha^{-1}) and the evapotranspiration (RMSE = 1.44 mm), where these observations were available (Alps). The model was applied under present and two climate datasets characterised by temperature increase and precipitation decrease (+2 °C temperature, -10 % precipitation) and reference or enriched CO_2 concentration (394 vs. 540.5 ppm) scenarios. The results showed that, while changes in temperature and precipitation alone had a negative impact by increasing NEE (+0.69 Mg C ha^{-1}) and decreasing total biomass (-0.20 Mg d.m. ha^{-1}) in the reference CO_2 scenario, the enriched atmospheric CO_2 concentration partially smoothed the NEE trend (+0.27 Mg C ha^{-1}) and increased total biomass (+0.60 Mg d.m. ha^{-1}) compared to the present period. It is concluded that the GRASSVISTOCK model represents a first step towards an integrated tool for estimating the performance of the agro-pastoral systems in terms of biomass production, water and carbon fluxes, in the face of ongoing climate change.

1. Introduction

Grasslands are terrestrial biomes that cover ~26 % of the Earth's surface and contribute to the provision of several ecosystem services (e.g. carbon sequestration, biomass production, biodiversity conservation, etc.; Dibari et al., 2021; FAO, 2019; Zhao et al., 2020). Due to their capacity to store carbon (~34 % of the global terrestrial carbon), these biomes play a key role in climate change mitigation (Wang et al., 2021).

* Corresponging author.
E-mail address: sergi.costafredaaumedes@unifi.it (S. Costafreda-Aumedes).

https://doi.org/10.1016/j.agrformet.2025.110486
Received 23 December 2023; Received in revised form 26 February 2025; Accepted 2 March 2025
Available online 22 March 2025

In particular, their potential to increase carbon sequestration (e.g. 0.47 Mg C ha^{-1} y^{-1}; Conant et al., 2017) is highly dependent on the system management (e.g. fertilisation, irrigation, grazing/sowing/mowing, etc.) and climate (Bai and Cotrufo, 2022; Mayel et al., 2021). In this context, global warming and the high environmental impact of grassland intensification management (e.g. overgrazing) are expected to limit or reverse (from carbon sink to source) the potential carbon sequestration capacity of these environments (Chabbi et al., 2023; Chang et al., 2021a).

For assessing the current carbon sequestration capacity of grasslands, to optimize farm management, and to identify new adaptation and mitigation strategies against climate change, biogeochemical models represent useful tools to simulate soil carbon turnover in agro-ecosystems (e.g. ICBM, Andren and Katterer, 1997; CENTURY, Parton et al., 1994; RothC, Coleman and Jenkinson, 1996; Brilli et al., 2017). These models are run at specific time steps (e.g. RothC was originally run at a monthly time step) and consider the decomposition rate of soil organic carbon (SOC), as affected by abiotic and biotic factors (soil moisture, temperature, vegetation cover and manure; Coleman and Jenkinson, 1996, Parton et al., 1994). However, some of these soil carbon models do not simulate the vegetation growth and litterfall during the growing season. Therefore, observations or *a priori* estimates of carbon litter are used as model inputs or to compare the results from model estimates, which in turn limits the spatial application and future predictions of these tools (Coleman and Jenkinson, 1996; Kaonga and Coleman, 2008). This limitation can be overcome by coupling a plant growth model with a soil carbon model to improve the simulation of daily grass biomass accumulation and leaf senescence (e.g. DAYCENT and PaSim with CENTURY submodel or DNDC; Li et al., 1992a,b; Parton et al., 1998; Riedo et al., 1998; Yin et al., 2020). In these models, simulations of plant growth and biomass accumulation, as affected by seasonal abiotic stresses (e.g. thermal and water stress), allow the dynamic of vegetation development, litterfall and root senescence to be taken into account, thereby improving estimates of carbon input to soil and ecosystem carbon fluxes. Thus, the integration of both approaches is expected to produce twofold advantages: (i) to improve the estimation of the plant senescent biomass, and (ii) to allow the simulation of the SOC turnover (Del Grosso et al., 2012).

The modelling solutions proposed so far have been shown to be able to simulate carbon fluxes, SOC and net accumulated biomass. When applied in a future climate, these tools may allow the evaluation of adaptation (i.e. reducing negative impacts on biomass accumulation) and mitigation strategies (i.e. increasing net ecosystem carbon uptake and/or soil carbon stocks; Bellini et al., 2023a; Brilli et al., 2023; Sándor et al., 2020; Zani et al., 2023) by considering the effects of agro-management practices (e.g. mowing, grazing, irrigation, etc.), which play a key role in vegetation growth and, consequently, in ecosystem carbon sequestration and emissions (Argenti et al., 2022). However, despite their good performance at simulating agro-pastoral systems (Brilli et al., 2023; Khalil et al., 2020; Sándor et al., 2020), the applicability of these models (e.g. DAYCENT, PasSim, DNDC) is still limited because they are not easy to parametrize. Indeed, the relatively high number of parameters (Laub et al., 2023; Rafique et al., 2015) and the detailed description of multiple processes (i.e. DAYCENT includes soil water balance, plant allocation, soil carbon turnover, nutrient mineralisation, N emission, CH_4 oxidation sub-models) increases the complexity of the model, its calibration and the uncertainty of the results (Barneze et al., 2022; Gurung et al., 2020; Necpálová et al., 2015). In an attempt to develop a simplified semi-mechanistic approach characterised by a simpler model structure (i.e. only biomass growth and water balance sub-models) and by limiting the number of parameters to be calibrated (less than 10), the VISTOCK model has recently proposed by Bellini et al. (2023b) to simulate grassland production. Taking advantage of this parsimonious architecture, the aim of this work was to extend the capability of the VISTOCK model to estimate carbon and water fluxes for the whole ecosystem. For this purpose, the original structure of the VISTOCK model was modified by replacing the remotely sensed NDVI-derived leaf area index (LAI) with a prognostic LAI simulation, which is the basis for estimating intercepted radiation, GPP, grass respiration and net biomass production on a daily time-step. Furthermore, this modified version of VISTOCK (GRASSVISTOCK) was coupled with a carbon model for SOC turnover (RothC; Coleman and Jenkinson, 1996) for a comprehensive estimation of the carbon fluxes from the system. GRASSVISTOCK was calibrated and tested to estimate the main grassland carbon fluxes (net ecosystem exchange, NEE; gross primary production, GPP and ecosystem respiration, RECO) and biomass accumulation in contrasting environments (from the Alps to the Mediterranean regions), taking into account the impact of the management practices (no management, periodic mowing). Finally, the calibrated version of the GRASSVISTOCK model was applied to the same testing sites under future climates in order to outline the possible consequences of a warmer and drier climate on NEE and biomass production in warm (Mediterranean) and cold (Alpine) regions.

2. Materials and methods

2.1. Study area

The study area includes three sites located across an altitudinal gradient in the Swiss (CH-Cha: 47.2102 °N, 8.4104 °E, 393 m), Austrian (AT-Neu: 47.1167 °N, 11.3175 °E, 970 m) and Italian (IT-Tor: 45.8444 °N, 7.5781 °E, 2160 m) Alpine chain. More specifically, CH-Cha, AT-Neu and IT-Tor sites are located in the hilly (300–800 m above sea level, a.s.l.), montane (800–1850 m a.s.l.) and sub-alpine (1500–2500 m a.s.l.) Alps elevation belt, respectively. On the other hand, the Mediterranean sites are located in central-northern Italy (S. Ilario and Bibbiano, renamed "S.Ilario": 44.6885 °N, 10.4781° E, ~97 m, on average for the five farms located in the area; Borgo San Lorenzo, renamed "Borgo": 43.9536 °N, 11.3487° E, 200 m; Marradi: 44.0810 °N, 11.6327° E, 600 m; Fig. 1). In particular, the S. Ilario site includes five farms (A: 44.6590°N, 10.4420°E; B: 44.7080°N, 10.4901°E; C: 44.6531°N, 10.4490°E; P: 44.7550°N, 10.4910°E; and S: 44.6660°N, 10.5170°E), located at a maximum distance of 12 km from each other and characterised by similar climate.

The climate in grasslands located in Alpine chain is temperate (CH-Cha), warm summer continental (AT-Neu) and intra-alpine semi-continental (IT-Tor; Table 1; Köppen, 1936; https://meta.icos-cp.eu/resources/stations/ES_IT-Tor; https://fluxnet.org/, Pastorello et al., 2020), with mean annual temperature and precipitation ranging from 2.9 °C (IT-Tor) to 9.5 °C (CH-Cha) and from 852 mm (AT-Neu) to 1136 (CH-Cha) mm, respectively (https://fluxnet.org/). Although characterized by different climates, we defined CH-Cha, AT-Neu and IT-Tor sites as "Alpine" by referring to their belonging to the Alpine chain and to distinguish them from the Mediterranean sites.

The Mediterranean sites, instead, are characterised by a transitional humid subtropical - Mediterranean climate with mean annual temperature and precipitation ranging from 12 °C (Marradi) to 14 °C (S.Ilario) and from 752 mm (S.Ilario) to 1330 mm (Marradi), respectively (Table 1; Bellini et al., 2023b; Köppen, 1936; https://www.arpae.it/).

All the study sites were characterised by different vegetation species composition and management practices. In particular, the vegetation of the managed CH-Cha and AT-Neu sites was characterized by a mixture of Italian ryegrass (*Lolium multiflorum*, Lam.), white clover (*Trifolium repens* L.; CH-Cha), and dominant graminoids (*Dactylis glomerata* L., *Festuca pratensis* Huds., *Phleum pratense* L., *Trisetum flavescens* L.), legumes (*Trifolium repens* L., *Trifolium pratense* L.) and forbs (*Ranunculus acris* L., *Taraxacum officinale*, G.H. Weber ex Wiggers, *Carum carvi* L.) species (AT-Neu). Conversely, the species composition of the unmanaged grassland of IT-Tor is characterised by *Nardus stricta* L. as the dominant vegetation, followed by *Poa alpina* L., *Trifolium alpinum* L., *Arnica montana* L. and *Ranunculus pyrenaeus* L. species. In the Mediterranean area, the farms located at S. Ilario site are characterised by

Fig. 1. Location of the study sites (CH-Cha, AT-Neu, IT-Tor, S.Ilario, Borgo and Marradi). The red circle around S. Ilario site is used for describing the area in which the five farms are located.

Table 1
Main features (Weather, Management, Soil) of the study sites. * Outliers have been removed. ** Avg. between 5 farms. *** Avg. of soil texture collected across 15 sites at 15–30 cm soil depth; Dal Prà et al. (2023).

Component	*Variable*	*Unit*	*Site*					
			CH-Cha	AT-Neu	IT-Tor	S. Ilario	Borgo (A & B)	Marradi
Weather	Latitude; Longitude	Decimal degrees	47.2102; 8.4104	47.1167; 11.3175	45.8444; 7.5781	44.6885; 10.4781**	43.9536; 11.3487	44.0810; 11.6327
	Altitude	m a.s.l.	393	970	2160	97**	200	600
	Period	Years	2005–2014*	2002–2012*	2012–2018	2017–2018	2020–2021	2020–2021
	Avg. Tmax	°C	34	31.6	21.9	37.75	38.2	34.5
	Avg. Tmin	°C	-13.75	-17.5	-16.7	-10.35	-6.3	-4.1
	Avg. Tmean	°C	9.8	7.4	3.6	13.9	13.9	13.1
	Annual Prec.	Mm	1136	666	914	672	924	1274
Management	Mowing	n. of avg. annual operations	5	3	–	5	1	1
	Grazing	Type; Avg. stocking rate, Animal ha^{-1}	Sheep; 24	–	–	–	Cattle; 1.43	Cattle; 3.5
		Avg. Period (months)	Apr and Nov	–	–	–	from Apr to Nov	from May to Aug
	Irrigation	Avg. water amount per operations; m^3	–	–	–	1877	–	–
		n. of avg. annual operations	–	–	–	5	–	–
Soil	Topsoil Soil Organic Carbon (SOC)	Mg C ha^{-1}	74.1 (30 cm)	78.83 (20 cm)	64.7 (20 cm)	–	79.87 (20 cm)	103.66 (20 cm)
	Bulk Density	g cm^{-3}	1.1	1.44	0.95	–	1.39	1.17
	Clay	%	21	5.24	13.07	37.8***	34.7	35.2
	Sand	%	46.3	53.05	45.2	10.3***	27.4	21.9
	Silt	%	32.7	41.71	41.73	52***	37.9	42.9

permanent grasslands, where the dominant vegetation is composed by Italian ryegrass (*Lolium multiflorum*, Lam.), white clover (*Trifolium repens*, L.) and other forbs (*Convolvulus arvensis*, L., *Taraxacum officinale*, G.H. Weber ex Wiggers). Finally, in the sown pastures of Borgo and Marradi sites the vegetation is mainly composed by graminoids (*Lolium* spp., *Dactylis glomerata* L., *Festuca arundinacea* Schreb., *Phleum pratense* L.), legumes (*Trifolium pratense* L., *Trifolium repens* L., *Lotus corniculatus* L., *Onobrychis viciifolia* Scop.) and forbs with the occasional presence of shrubs (mainly *Rubus ulmifolius* Schott).

The agronomic practices applied in the Alpine area were characterised by mowing (CH-Cha and AT-Neu) and seasonal sheep grazing (CH-Cha), while no management practices were applied in IT-Tor. In the Mediterranean area, the management practices applied in S.Ilario were mainly characterised by mowing and irrigation (surface flooding and sprinklers; Dal Prà et al., 2023). Finally, Borgo and Marradi sites were characterised by mowing and beef cattle grazing, with Borgo being characterised by two areas with different management (A and B; Bellini et al., 2023b).

In terms of soil conditions, the three Alpine sites were classified as sandy loam soils (Table 1; Pintaldi et al., 2016; Wohlfahrt et al., 2008;

Feigenwinter et al., 2023). The five farms in S.Ilario site were characterised by silty clay loam texture at 15–30 cm soil depth (Table 1; Dal Prà et al., 2023). Considering the similar pedo-climatic conditions of the five farms in S.Ilario, they were all considered as a single unit and jointly calibrated. However, the specific agronomic practices were applied according to the schedule of each farm. Finally, Borgo and Marradi showed clay loam soil characteristics (Table 1; Bellini et al., 2023b). Specifically, the weather, management and soil conditions of the sites are reported in Table 1.

2.2. Observed data

Daily observed weather data (air temperature, °C; precipitation, mm and global solar radiation, MJ m^{-2} d^{-1}), the vapor pressure deficit (VPD, hPa) and daily eddy covariance (EC) measurements (NEE, g C m^{-2} d^{-1}; GPP, g C m^{-2} d^{-1} and RECO, g C m^{-2} d^{-1}) for CH-Cha (2005–2014), AT-Neu (2002–2012) and IT-Tor (2012–2018) sites were collected from the FLUXNET dataset (Baldocchi et al., 2001; Pastorello et al., 2020; https://fluxnet.org/). The reference values of NEE, GPP and RECO (g C m^{-2} d^{-1}), based on a variable threshold of friction velocity (u_*; VUT_REF) and the nighttime method (NT), were selected as reference observed data in all three Alpine sites (Pastorello et al., 2020; Reichstein et al., 2005). The NEE, GPP and RECO values were then converted from g C m^{-2} d^{-1} to Mg C ha^{-1}, and unreliable observations were removed from the datasets (e.g. NA values and/or according to the quality control flag, available in FLUXNET dataset, Pastorello et al., 2020). On the other hand, maximum and minimum air temperature (°C) were extracted from the hourly temperature of the FLUXNET dataset, while the daily snow cover data (0 = no snow cover; 1 = snow cover) was simulated using the snowMAUS model (Trnka et al., 2010), for all datasets except for the IT-Tor, where this information was included by the data provider.

For the Mediterranean sites, the daily weather data (maximum and minimum air temperature, °C and precipitation, mm) of the closest weather stations in S.Ilario area were collected from Dext3r web application of the Arpae-Simc regional service of Emilia-Romagna during the period 2017–2018 (https://simc.arpae.it/dext3r/). For this site, the daily global solar radiation (MJ m^{-2} d^{-1}) was estimated using the Hargreaves method (Hargreaves and Samani, 1982). Finally, the daily weather data (maximum and minimum air temperature, °C and precipitation, mm) for Borgo and Marradi sites were collected during 2020–2021 from Servizio Idrologico Regionale of Tuscany region dataset (SIR, https://www.sir.toscana.it/), and the daily global solar radiation (MJ m^{-2} d^{-1}) was estimated by Bellini et al. (2023b) based on the approach proposed by Bristow and Campbell (1984) in the "sirad" package in R software (Bojanowski, 2016).

Leaf area index (LAI; m^2 m^{-2}), above-ground biomass (AGB; g d.m. m^{-2}) and soil water content (SWC, m^3 m^{-3}) measurements were available for both Alpine and Mediterranean sites. LAI data were obtained for CH-Cha (2010–2011; https://fluxnet.org/), AT-Neu (2002–2006; Wohlfahrt et al., 2008), IT-Tor (2012–2018; Filippa et al., 2015), Borgo A and B and Marradi (2020–2021; Bellini et al., 2023b) sites, while AGB data were collected for CH-Cha (2009–2011; https://fluxnet.org/), IT-Tor (2012–2018; Filippa et al., 2015), S. Ilario (amount of biomass obtained from each cut in 2017–2018; Dal Prà et al., 2023) and Borgo A and B and Marradi (2020–2021; Bellini et al., 2023b). Additionally, the SWC data were measured with Theta probe M1, Delta-T, UK in AT-Neu (2002–2012) and with CS-616, Campbell Scientific in IT-Tor (2012–2018) sites (https://fluxnet.org/; Bellini et al., 2023b). The SWC data were used for deriving fractional transpirable soil water (FTSW, the ratio between the actual water content and total transpirable soil water) at daily time step. Soil organic carbon content (SOC) measurements were derived from total organic carbon (TOC, g kg^{-1}) and soil organic matter (SOM, %) and quantified in 74.1 Mg C ha^{-1} at 30 cm in CH-Cha, 78.3 Mg C ha^{-1} at 20 cm in AT-Neu and 64.7 Mg C ha^{-1} at 20 cm in IT-Tor (Feigenwinter et al., 2023; Pintaldi et al., 2016; Seeber et al., 2022). Finally, SOC ranged from 79.87 Mg C ha^{-1} to 103.66 Mg C ha^{-1} in Borgo and Marradi sites (https://soilgrids.org, Poggio et al., 2021; Table 1).

2.3. Model description

GRASSVISTOCK is a semi-mechanistic model which explicitly simulates grass growth and daily LAI dynamic, biomass accumulation and partitioning, including water and carbon fluxes of agro-pastoral systems. This model represents a modified version of the original VISTOCK model (Bellini et al., 2023b), a diagnostic model where LAI is derived from Normalized Difference Vegetation (NDVI; Rouse et al., 1974). In this new version, an alternative modeling strategy was implemented for simulating LAI development.

For each day, the net increase in LAI (the green LAI, GLAI, m^2 m^{-2} d^{-1}) is calculated as the difference between the daily LAI growth rate (LAI_{rate}, m^2 m^{-2} d^{-1}) and the senescent LAI (LAI_{sen}, m^2 m^{-2} d^{-1}; Eq.1).

$$GLAI = LAI_{rate} - LAI_{sen} \quad (1)$$

LAI_{rate} (Eq. (2)) is calculated considering the Net Primary Production (NPP; g m^{-2} d^{-1}) partitioned according to a coefficient (LAI_{part}) and the ratio of leaf area to dry mass (specific leaf area, SLA, m^2 g^{-1}; assuming that the entire AGB is invested in leaf area):

$$LAI_{rate} = NPP \cdot LAI_{part} \cdot SLA \quad (2)$$

Accordingly, total LAI (LAI_{grass}, m^2 m^{-2}) of a specific period is calculated as daily accumulation of GLAI from the beginning of the simulation until the end of the considered period (Eq. 3).

$$LAI_{grass} = \sum_{1}^{n} GLAI \quad (3)$$

The NPP is partitioned to AGB according to the coefficient BIO_{part} ($LAI_{part} = BIO_{part}$) while the daily below ground biomass (BGB, g m^{-2} d^{-1}) is calculated according to Eq. 4.

$$BGB = NPP \cdot (1 - BIO_{part}) \quad (4)$$

A fixed turnover factor was applied to BGB in order to simulate the amount of senescent matter (Table 2).

The NPP is calculated as the difference between gross primary production (GPP; gC m^{-2} d^{-1}) and autotrophic respiration (R_a; gC m^{-2} d^{-1}) and then converted from gC m^{-2} d^{-1} to g d.m. m^{-2} d^{-1}. GPP is dependent on the amount of photosynthetically active radiation (PAR, MJ d^{-1}) intercepted by LAI (fraction of the photosynthetically active radiation, fPAR) and a conversion factor of daily intercepted PAR to carbon assimilation (maximum radiation use efficiency, ε_{maxref}; g C MJ^{-1}). Thermal and water stress factors (T_{cor} and WS_{cor}; Maselli et al., 2013; Veroustraete et al., 2004), and snow cover (SNOW) are scalars to reduce maximum potential to actual radiation use efficiency (Eq. 5).

$$GPP = \varepsilon_{maxref} \cdot PAR \cdot fPAR \cdot T_{cor} \cdot WS_{cor} \cdot SNOW \quad (5)$$

fPAR is estimated through the Beer's Law equation based on light extinction coefficient for vegetation cover here described by LAI_{grass} (Sinclair, 2006; Bellini et al., 2023b).

T_{cor} is a scalar that ranges from 0, GT_{min} (no vegetation growth), to 1, GT_{opt} (optimal vegetation growth; Heinsch et al., 2003; Eqs. 6 and 6.1) depending on daily minimum temperature.

$$T_{cor} = a \cdot T_{min} + b \quad (6)$$

$$T_{cor} = \begin{cases} 0 & T_{cor} < 0 \\ T_{cor} & 0 \le T_{cor} \le 1 \\ 1 & T_{cor} > 1 \end{cases} \quad (6.1)$$

Similarly, WS_{cor} is a water stress factor calculated from the soil water balance module. The soil water balance is simulated on a soil module composed by two layers. In these layers, the soil water dynamic is described by considering the water content availability (WCA, i.e., water

Table 2
GRASSVISTOCK model parameter list for all study sites. In bold, the values were the same for all sites.

Parameter	CH-Cha	AT-Neu	IT-Tor	S.Ilario	Borgo A and B	Marradi	Unit
GRASSVISTOCK model							
Leaf area seasonal dynamics							
$LAIgrass_{ini}$	0.8	0.8	0.2	2	0.25, 0.5	0.3	$m^2\ m^{-2}$
$Leaf_{Life}$	230	450	164	500	312	200	°C days
$LAI_{Life.ini}$			**3500**				°C days
$LAI_{stop.sen}$	0.9	0.5	0.5	1.5	0.5	0.5	$m^2\ m^{-2}$
LAI_{min}	0.8	0.8	0.1	0.5	0.05	0.05	$m^2\ m^{-2}$
LAI_{part}			**50**				%
SLA[1]	0.021	0.021	0.019	0.021	0.021	0.021	$m^2\ g^{-1}$
Light interception and Biomass accumulation							
eP^2_{maxref}			**1.65**				$g\ C\ MJ^{-1}$
GT^3_{min}	-7	-8	-6.13	-6.47	-3	5	°C
GT^3_{opt}	1	0.5	12	3.5	12	11.8	°C
A			**9.49**				–
B			**15.69**				–
TEC_{ref}			**4.5**				Pa
$cumAGB_{t0}$	100	50	100	100	50, 190	70	$g\ m^{-2}$
$cumBGB_{t0}$	2800	3000	1200	2500	600	1000	$g\ m^{-2}$
Y^4_g			**0.75**				–
k^5_m	0.0008	0.0003	0.0003		0.0006		d^{-1}
Bio_{part}			**50**				%
$Root_{sen}$	**30**						%
$CO2_{ref}$			**394**				ppm
b1			**0.2**				–
b2			**0.26**				–
Soil characteristics and Water balance							
SoilDepth	125	100	100	150	80	80	cm
RootDepth	60	60	50	70	50	60	cm
SoilCDepth	30	20	20	20	20	20	cm
EDEP	30	20	20	20	20	20	cm
WCA	0.2	0.18	0.15	0.2	0.15	0.16	–
AWAFC			**2**				cm
VPDF	0.35	0.35	0.65	0.56	0.4	0.5	–
sALB			**0.9**				–
$FTSW_{thr}$			**0.35**				–
$PREC_{thr}$			**6**				mm
Roth C							
Clay	21	5.24	13.07	36*	34.7	35.2	%
DR[6]	1.44	1.44	0.67	1.44	1.44	1.44	–
k^7_{DPM}			**10****				y^{-1}
k^7_{RPM}			**0.3****				y^{-1}
k^7_{HUM}			**0.02****				y^{-1}
k^7_{BIO}			**0.66****				y^{-1}
k^7_{IOM}			**0****				y^{-1}
pE			**1**				–

References: [1]Porter and De Jong (1999); [2]Maselli et al. (2013); [3]Running and Zhao (2019); [4]Thornley and Cannell (2000); [5]Amthor (1984); [6]Coleman and Jenkinson (1996); [7]Jenkinson et al. (1987, 1992). *Average clay values in S.Ilario: A: 38.2 %, B: 36.8 %, C: 32.3 %, P: 37.8 %, S: 34.7 %.**The annual decomposition rates have been rescaled at daily time step.

potentially available between field capacity and wilting point, $m^3\ m^{-3}$), the Total Transpirable Soil Water (TTSW; i.e. WCA * rooting depth, mm) and the Available Transpirable Soil Water (ATSW, mm; i.e. the amount of water really available to the plant). The ratio between ATSW and TTSW, defined as Fraction of Transpirable Soil Water (FTSW, unitless), which ranges from 0 (no water available for transpiration) to 1 (potential water conditions) is used for WS_{cor} calculation as limiting factor for GPP (Eqs. 7, 7.1). More details on this general framework can be found in Sinclair (1986), Bindi et al. (2005), Soltani and Sinclair (2012), Moriondo et al. (2019) and Bellini et al. (2023b).

$$WS_{cor} = \frac{1}{1 + a \cdot e^{(b \cdot FTSW_g)}} \tag{7}$$

$$WS_{cor} = \begin{cases} 0 & WS_{cor} < 0 \\ WS_{cor} & 0 \le WS_{cor} \le 1 \\ 1 & WS_{cor} > 1 \end{cases} \tag{7.1}$$

ATSW is updated at the end of the day, based on its value on the previous day and the positive (precipitation and irrigation; mm) and negative (soil evaporation SEVP and plant transpiration TR, mm) budget items (Eq. 8).

$$ATSW_d = ATSW_{d-1} + (Precipitation + Irrigation) - (\mathrm{SEVP} + \mathrm{TR}) \tag{8}$$

Plant transpiration is estimated considering the existing relationship with plant assimilation (Tanner and Sinclair, 1983; Soltani and Sinclair, 2012; Eqs. 9, 9.1)

$$TR = \frac{GPP}{TE} \tag{9}$$

$$TE = \frac{TEC_{ref}}{VPD} \tag{9.1}$$

where TR is daily plant transpiration (mm d^{-1}), TE is transpiration efficiency which depends on VPD and transpiration efficiency coefficient

(TEC_{ref}, Pa) that is species dependent. The soil potential evaporation ($SEVP_{pot}$) is calculated using the Penman equation reported in Soltani and Sinclair (2012; Eqs. 10, 10.1).

$$SEVP_{pot} = GSR \cdot SALB \cdot (1 - fPAR) \cdot \frac{DELT}{DELT + 0.68} \quad (10)$$

$$DELT = \frac{5304}{(273 + Tmax)^2} \cdot e^{\left(\frac{21.255 - 5304}{273 + Tmax}\right)} \quad (10.1)$$

Where DELT is the slope of saturated vapor pressure versus temperature for daily temperature calculated according to Soltani and Sinclair (2012), GSR is the daily incident solar radiation (MJ m^{-2} d^{-1}), SALB is the soil albedo and fPAR is the grass intercepted radiation.

When FTSW is lower than a specific threshold ($FTSW_{THR}$), SEVPpot is rescaled to actual SEVP as a function of the square root of time since the start of the dry spell (DYSE, days) by considering that the evaporation in the grass soil layer is different from a wet surface ($SEVP_{pot}$; Eq. 11).

$$SEVP = SEVP_{pot} \cdot \left(\sqrt{DYSE + 1}\right) - \sqrt{DYSE} \quad (11)$$

Moreover, GRASSVISTOCK accounts for the effect of CO_2 atmospheric concentration (ppm) on photosynthesis (ε_{maxref}) and transpiration efficiency coefficient (TEC_{ref}) according to the approach proposed by Soltani and Sinclair (2012) and Kellner et al. (2017; Eqs. 13-14):

$$\varepsilon_{\max CO_2} = \varepsilon_{\max ref} \cdot \left[1.0 + b1 \cdot \ln\left(\frac{CO_{2meas}}{CO_{2ref}}\right)\right] \quad (13)$$

$$TEC_{CO_2} = TEC_{ref} \cdot \left[1.0 + b2 \cdot \ln\left(\frac{CO_{2meas}}{CO_{2ref}}\right)\right] \quad (14)$$

Where ε_{maxCO2} and TEC_{CO2} are the maximum radiation use efficiency and the transpiration efficiency coefficients, as affected by atmospheric CO_2 concentration (the so-called "CO_2 fertilization effect"), respectively. ε_{maxref} and TEC_{ref} are the maximum radiation use efficiency and the transpiration efficiency coefficient at reference atmospheric CO_2 concentration (394 ppm). b1 and b2 are the coefficients regulating the response of the ε_{maxref} and TEC_{ref} to CO_2, respectively. CO_{2meas} and CO_{2ref} are the measured and the reference atmospheric CO_2 concentration values (ppm), respectively. b1 was set following Kellner et al. (2017) for assessing the impact of CO_2 on ε_{maxref} while b2 was calibrated considering the increase of WUE under elevated CO_2 concentrations as described in the same study of Kellner et al. (2017).

The plant respiration (R_a, gC m^{-2} d^{-1}) is estimated following the 'growth-maintenance respiration paradigm' (GMRP) of Thornley and Cannell (2000; Eqs. 15-17):

$$R_a = R_g + R_m \quad (15)$$

$$R_g = (1 - Y_g) \cdot (GPP - K_m \cdot BIO_{tot}) \quad (16)$$

$$R_m = K_m \cdot BIO_{tot} \quad (17)$$

Where R_g and R_m are the growth and maintenance respiration, respectively. Y_g is the growth yield (kg structural C · kg substrate C^{-1}), K_m is the maintenance coefficient (d^{-1}) and BIO_{tot} is the total dry mass (gC m^{-2}).

Mowing, grazing and irrigation events were included in the simulations according to the relevant information provided for each site. For AT-Neu and CH-Cha sites, the mowing was simulated according to the information indicated in the "mowing management file", which reports the year, day of year (DOY) and reduction (%) in LAI and AGB.

Similarly, grazing is applied according to the information reported in the "grazing management file" (Year, DOY_{ini}, DOY_{end}, Stocking rate, potential and actual feeding), where AGB reduction during the grazing period (DOY_{ini} and DOY_{end}) was achieved by considering the stocking rate (animal m^{-2}) and the daily dry matter biomass intake of the animals (g animal^{-1} d^{-1}; actual feeding). The difference between potential and actual feeding was determined by the decrease of animal feeding in the pasture, and the eventual integrations for supporting animal diet during the season. Finally, irrigation is applied following the information provided in the "irrigation management file" (Year, DOY and Water Amount, mm), which allows simulating the effect of the prompt water input on soil water content during the season. The information about management is reported in Table 1.

To account for soil carbon dynamics, GRASSVISTOCK model was integrated with the RothC soil model (Coleman and Jenkinson, 1996) as available in SoilR package for the R software environment (v. 4.2.2, R Core Team 2022; Sierra et al., 2012; Fig. 2). The original version of RothC model was developed for simulating the soil organic carbon turnover at monthly time step by considering the temperature and moisture effects, soil type and plant cover. In the RothC model the organic carbon (Mg C ha^{-1}) is decomposed in four active pools (DPM = Decomposable Plant Material; RPM = Resistant Plant Material; BIO = Microbial Biomass; HUM = Humified Organic Matter) and one inert pool (IOM = Inert Organic Matter) following first-order kinetic processes (Coleman and Jenkinson, 1996). To harmonize the time resolution of GRASSVISTOCK (daily) and RothC (monthly), the timescale of the original version of RothC was converted from monthly to daily time step by re-scaling the original decomposition rate values of each pool. Accordingly, GRASSVISTOCK interfaces with RothC providing on a daily basis daily average air temperature (°C), precipitation (mm) and evapotranspiration (mm) to simulate the temperature and moisture impacts on soil carbon decomposition and the daily fraction of litter C (Mg C ha^{-1}), which was estimated by GRASSVISTOCK as dependent on senescence of AGB and BGB. The DPM/RPM ratio of the incoming material was set to 1.44 (CH-Cha and AT-Neu) and to 0.67 (IT-Tor) as required for improved and unimproved grasslands (Coleman and Jenkinson, 1996). The main outputs of the Roth C model were soil carbon fluxes (Mg C ha^{-1} d^{-1}).

The modeled soil respiration was used, together with modeled plant respiration, for estimating RECO (Eq. 18; Mg C ha^{-1} d^{-1}), which then was compared to the RECO partitioned from measured NEE (Mg C ha^{-1} d^{-1}; Eq. 19).

$$RECO = R_h + R_a \quad (18)$$

$$NEE = RECO - GPP \quad (19)$$

Where positive NEE values refer to net CO_2 emissions while negative NEE values results in net CO_2 uptake of the system.

2.4. Model calibration and evaluation

The GRASSVISTOCK model calibration was performed by using the CroptimizR package within the R software environment (version 4.2.2., R Core Team, 2021; Buis et al., 2020).

The calibration procedure was carried out considering the "crit_log_cwss" criteria based on the log transformation of the concentrated version of weighted sum of squares, described in Wallach et al. (2011). The calibration follows the scheme described in Fig. S1. To assess the importance of individual variables in model optimization, some model calibrations (here called tests for distinguishing them from site specific calibrations) were initially performed at IT-Tor site, where most of the observed variables (NEE, AGB, LAI and SOC data) were available. At this site, the tests were performed using the combination of different observed variables: 1st test was performed using all available obesrved variables, i.e. NEE, LAI, AGB and initial soil C pool; 2nd test was performed using NEE, LAI and AGB observed variables and 3rd test was performed using LAI and AGB variables. While the *t*-test statistic evidenced in any case significant differences among simulated and observed values, no significant differences were observed when comparing the tests among them (Fig. S1), implying that optimization can still occur with the minimum observed dataset, i.e. LAI and AGB.

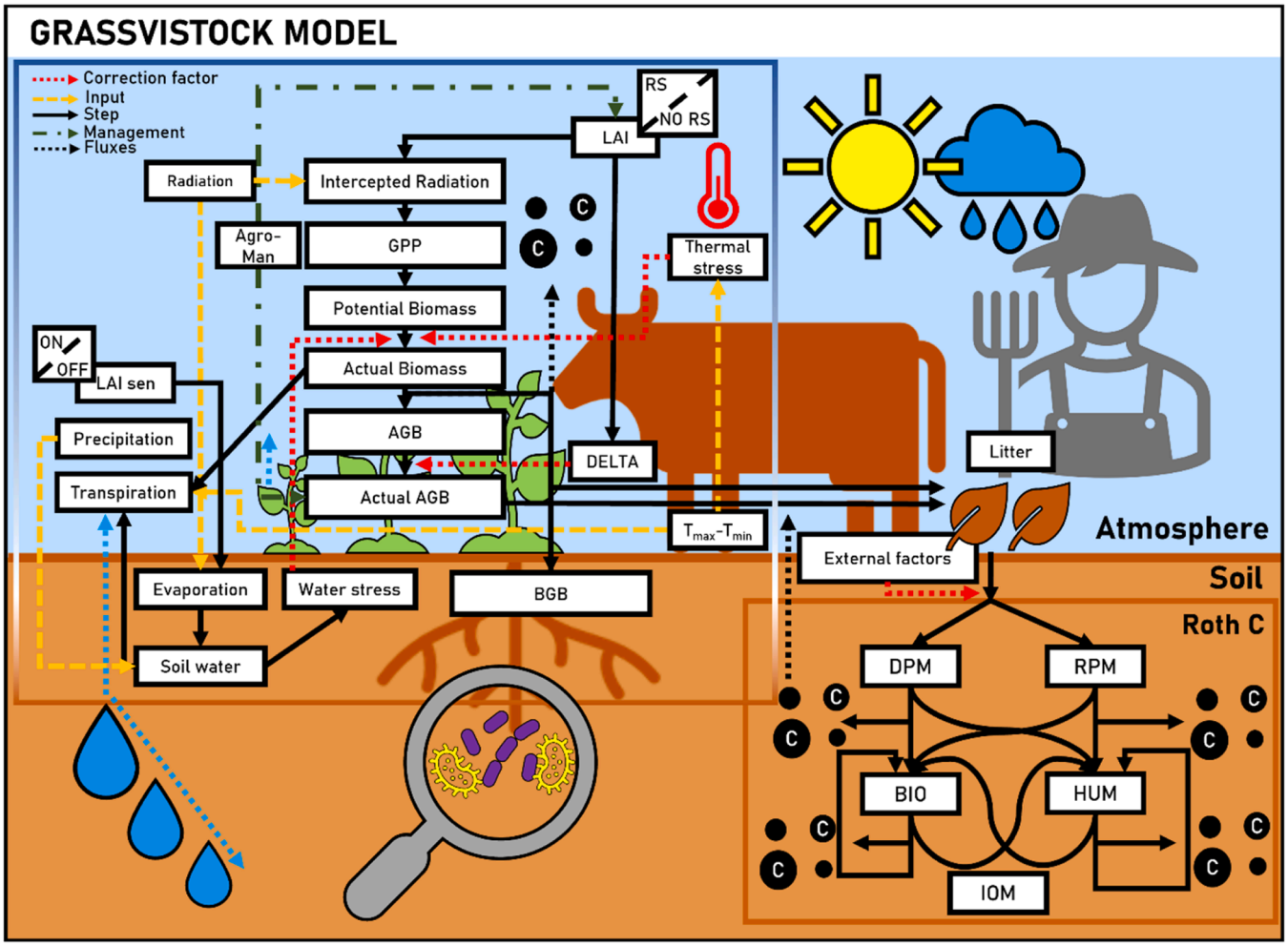

Fig. 2. Model workflow: description of the modeled physiological processes for representing daily grass growth dynamics (LAI, AGB and BGB), soil water balance and organic carbon turnover using the Roth C module. The GRASSVISTOCK provides an alternative strategy to the diagnostic approach of the original model version of Bellini et al. (2023b; RS-derived LAI), by implementing the prognostic model approach for simulating LAI dynamics (NO RS). The new model also includes the impact of agro-management practices (e.g. irrigation, mowing and grazing) on LAI and biomass accumulation. The external factors affecting soil carbon decomposition are: abiotic stress (temperature and soil water content and vegetation cover). LAI = Leaf Area Index; AGB = Above Ground Biomass; BGB = Below Ground Biomass; GPP = Gross Primary Production; RS = Remote Sensing; DPM = Decomposable Plant Material; RPM = Resistant Plant Material; BIO = Microbial Biomass; HUM = Humified Organic Matter; IOM = Inert Organic Matter.

Subsequently, GRASSVISTOCK model was calibrated by considering the data availability (NEE, LAI and/or AGB) for each site (e.g. the model calibration was exclusively performed on LAI and/or AGB where NEE observations were not available such as in Mediterranean sites).

The model parameters selected for model calibration and the range of parameters values is described in Table S1. During the model calibration, the value of most of the parameters was defined by literature and kept constant among sites. For example, BIO_{part} was set to 50 % considering the fact that assimilated carbon is equally distributed between AGB and BGB (Xu et al., 2013). BGB senescence rate was set to 30 % according to (Wang et al., 2019b; Garcia-Pausas et al., 2011). On the other hand, only few parameters were calibrated as they were related to site-specific conditions (Table 2).

A model spin-up was performed in order to identify the initial content of the soil pools (i.e. DPM, RPM, BIO, HUM and IOM). Initially, the fraction of total SOC in each pool (%) was defined according to the values established in the literature (Xu et al., 2011; Zimmermann et al., 2007). The model was then run for 500 years on each site trying to maintain the equilibrium conditions of each pool. In the event that the model did not reach equilibrium, the contents of the soil C pool were redefined by varying the partitioning percentage in each pool by 20 % from the values found in the literature.

Finally, the model evaluation was performed on the GPP, RECO and ET estimates retrieved from the FLUXNET dataset (https://fluxnet.org/; Data accessed: 01/12/2023).

2.5. Model application in a future climate scenario

To simulate future meteorological data, a delta change approach (Arnell, 1996) was applied to modify original observed meteorological data of the study sites, where a constant daily increase of 2 °C of temperature and a decrease of 10 % for each precipitation event was applied to the relevant datasets. These variations were considered because consistent with the RCP8.5 climate scenario of IPCC (IPCC, 2014; Moss et al., 2010), reflecting the mean annual temperature and precipitation anomalies expected around 2050 for the Mediterranean basin (Cherif et al., 2020) and leading the Mediterranean area to become an "Hot-Spot" (Noce et al., 2016). The reference atmospheric CO_2 concentration was set at 394 ppm during the present period (Kellner et al., 2017), and in agreement with the trend in atmospheric CO_2 concentrations (ppm) from 2002 to 2018 (389.35±10.84 ppm; https://www.eea.europa.eu/). For reproducing the future scenario, the atmospheric CO_2 concentration was set to 540.5 ppm according to the RCP8.5 scenario in 2050 (IPCC, 2013).

The GRASSVISTOCK model was thus run with the present and the new climate dataset (+2 °C temperature, -10 % precipitation, 540.5 ppm), and the NEE, GPP, RECO and ET trends were analyzed across all Alpine and Mediterranean sites.

2.6. Statistical analysis

The statistical analysis between observed and simulated results was performed considering Pearson's correlation coefficient (r, Eq. 20), the root mean squared error (RMSE, Eq. 21), the mean absolute error (MAE, Eq. 22), the normalized root mean squared error (NRMSE, Eq. 23), normalized on the difference on the range of observed values, the Nash-Sutcliffe modelling efficiency (EF, Eq. 24), the coefficient of residual mass (CRM, Eq. 25) and the percent bias (pBIAS, Eq. 26).

$$r = \frac{\sum_{i=1}^{n}(O_i - \overline{O})\cdot(P_i - \overline{P})}{\sqrt{\sum_{i=1}^{n}(O_i - \overline{O})^2 \cdot \sum_{i=1}^{n}(P_i - \overline{P})^2}} \quad (20)$$

$$RMSE = \sqrt{\sum_{i=1}^{n}\frac{(P_i - O_i)^2}{n}} \quad (21)$$

$$MAE = \frac{1}{n}\sum_{i=1}^{n}|O_i - P_i| \quad (22)$$

$$NRMSE = \frac{\sqrt{\sum_{i=1}^{n}\frac{(P_i - O_i)^2}{n}}}{O_{max} - O_{min}}\cdot 100 \quad (23)$$

$$EF = 1 - \frac{\sum_{i=1}^{n}(O_i - P_i)^2}{\sum_{i=1}^{n}(O_i - \overline{O})^2} \quad (24)$$

$$CRM = \frac{\sum_{i=1}^{n}O_i - \sum_{i=1}^{n}P_i}{\sum_{i=1}^{n}O_i} \quad (25)$$

$$pBIAS = 100\frac{\sum_{i=1}^{n}(P_i - O_i)}{\sum_{i=1}^{n}O_i} \quad (26)$$

Where O_i is the observed value, O is the average of the observed values, P_i is the predicted value, P is the average of the predicted values, and n is the number of observations. Regarding pBIAS equation, positive values indicate overestimation bias, while negative values indicates underestimation bias. The two-side *t*-test approach was performed by using the *t.test* function in the "stat" package of R software (R Core Team, 2021) and it was used for comparing observed and simulated results from different calibration procedures in IT-Tor (see following Results section).

3. Results

3.1. Model calibration and evaluation

The list of GRASSVISTOCK model parameters for all sites is reported in Table 2, while the parameters' description, information on calibrated parameters and the range of variation are reported in Table S1.

Only the coefficients regulating LAI development and limiting growth were locally calibrated to differentiate the grass growth dynamics between different environments and plant communities (Table S1). Mid-elevation Alpine sites CH-Cha (393 m a.s.l.) and AT-Neu (970 m a.s.l) exhibited a relatively similar set of parameters for GT_{min} and GT_{opt} (CH-Cha: GT_{min} = -7 °C; GT_{opt} = 1 °C; AT-Neu; GT_{min} = -8 °C; GT_{opt} = 0.5 °C), while the leaf duration $Leaf_{Life}$ was higher in AT-Neu (450 °C days) compared to CH-Cha (230 °C days).

The calibration for the five farms of S.Ilario, located in Emilia-Romagna region (Italy), resulted in a higher degree days accumulation and higher optimal temperature requirements for grass growth with respect to northern sites (S.Ilario: $Leaf_{Life}$ = 500 °C days; GT_{min} = -6.47 °C; GT_{opt} = 3.5 °C).

Southern sites in Borgo and Marradi showed similar grass growth trends, with higher temperature requirements for minimum growth found in Marradi compared to Borgo (Borgo: $Leaf_{Life}$ = 312 °C days; GT_{min} = -3 °C; GT_{opt} = 12 °C; Marradi: $Leaf_{Life}$ = 200 °C days; GT_{min} = 5 °C; GT_{opt} = 11.8 °C; Tables 1 and 2; Fig. S2).

As an exception to this trend, the high elevation Alpine site IT-Tor (2160 m asl) evidenced intermediate traits between mid-elevation Alpine and high elevation Alpine sites with $Leaf_{Life}$=164 °C days, GT_{opt} = 12 °C and GT_{min} = -6.13 °C.

As a first step for evaluating the LAI strategy performances, the prognostic LAI approach implemented in the new GRASSVISTOCK model was compared with the original diagnostic LAI strategy of VISTOCK model version for the simulation of LAI and AGB variables in IT-Tor site (Fig. S4). The remote sensing based approach (diagnostic strategy) showed better performances with respect to the prognostic approach when both LAI and AGB simulations were compared with observations (LAI: r = 0.76, RMSE = 0.41 m^2 m^{-2}; AGB: r = 0.83, RMSE = 42.55 g d.m. m^{-2}). Moreover, the overall performances in LAI and AGB simulations (Tables 3 and S2, Figs. 3 and S3) showed that high Pearson's correlation coefficients were obtained in all sites, with better results obtained, on average, in Borgo for LAI (0.91) and AGB (0.84) compared to AT-Neu (0.63) and IT-Tor (0.68) for LAI and AGB, respectively. This statistic was associated with a RMSE ranging from 0.79 m^2 m^{-2} (min in Borgo A) to 1.42 m^2 m^{-2} (max in Borgo B) for LAI and from 56.25 g d.m. m^{-2} (min in Borgo A) to 78.43 g d.m. m^{-2} (max in Borgo B) for AGB. On the other hand, the lowest RMSE performances were found in AT-Neu (2.68 m^2 m^{-2}) and S.Ilario (175.88 g m^{-2}) for LAI and AGB, respectively. According to the statistics presented in Table S2, better average model performances were obtained for AGB compared to LAI. In particular, IT-Tor showed the best performances considering both NRMSE (LAI = 31.60 %, AGB = 25.71 %) and pBIAS (LAI = -9.61

Table 3
Performance statistics of NEE (Mg C ha^{-1}), GPP (Mg C ha^{-1}), RECO (Mg C ha^{-1}), ET (mm), LAI (m^2 m^{-2}) and AGB (Mg d.m. ha^{-1}) across all study sites. Regarding fluxes, the statistics in the table refer to the complete datasets.

Site	Statistics	NEE Mg C ha^{-1}	GPP Mg C ha^{-1}	RECO Mg C ha^{-1}	ET mm	LAI m^2 m^{-2}	AGB Mg d.m. ha^{-1}
CH-Cha	r	0.35	0.71	0.61	0.80	0.73	0.74
	RMSE	0.04	0.04	0.04	1.58	1.40	1.29
	Slope	0.36	0.70	0.39	1.22	0.51	0.75
	Intercept	-0.006	0.007	0.02	0.08	0.77	-0.36
AT-Neu	r	0.27	0.71	0.55	0.69	0.63	–
	RMSE	0.04	0.05	0.05	1.37	2.98	–
	Slope	0.32	0.56	0.40	0.95	1.15	–
	Intercept	-0.002	0.01	0.02	0.55	0.009	–
IT-Tor	r	0.60	0.85	0.65	0.59	0.76	0.68
	RMSE	0.02	0.02	0.02	1.37	0.82	0.73
	Slope	0.56	0.82	0.80	0.56	0.96	0.85
	Intercept	0.0006	0.001	0.003	0.58	0.68	0.62
S. Ilario	r	–	–	–	–	–	0.72
	RMSE	–	–	–	–	–	1.76
	Slope	–	–	–	–	–	0.55
	Intercept	–	–	–	–	–	0.50
Borgo A	r	–	–	–	–	0.95	0.80
	RMSE	–	–	–	–	0.79	0.56
	Slope	–	–	–	–	1.35	1.45
	Intercept	–	–	–	–	0.36	0.08
Borgo B	r	–	–	–	–	0.88	0.85
	RMSE	–	–	–	–	1.42	0.78
	Slope	–	–	–	–	1.16	1.60
	Intercept	–	–	–	–	0.91	-0.21
Marradi	r	–	–	–	–	0.83	0.79
	RMSE	–	–	–	–	0.50	0.51
	Slope	–	–	–	–	1.31	0.66
	Intercept	–	–	–	–	-0.58	-0.06

Table 4
Average seasonal peak of AGB (Mg d.m. ha^{-1}), Average total AGB (Mg d.m. ha^{-1}) and annual average values of NEE (Mg C ha^{-1}), GPP (Mg C ha^{-1}), RECO (Mg C ha^{-1}) and ET (mm) under present period (0 °C temperature, 0 % precipitation, 394 ppm atmospheric CO_2 concentration) and modified climates (+2 °C temperature, -10 % precipitation, 394 ppm atmospheric CO_2 concentration; +2 °C temperature, -10 % precipitation, 540.5 ppm atmospheric CO_2 concentration). In brackets, the delta changes of the variables compared to the present period (0 °C temperature, 0 % precipitation, 394 ppm atmospheric CO_2 concentration.

Scenario	Site	Peak AGB (Mg d.m. ha^{-1})	Tot AGB (Mg d.m. ha^{-1})	NEE (Mg C ha^{-1})	GPP (Mg C ha^{-1})	RECO (Mg C ha^{-1})	ET (mm)
0 °C 0 % 394 ppm	CH-Cha	4.29	13.51	-3.64	21.28	17.64	881.33
	AT-Neu	6.05	12.57	0.64	16.98	17.62	633.79
	IT-Tor	3.43	5.54	-0.002	7.46	7.45	503.75
	S.Ilario (A)	3.88	9.79	-5.15	14.90	9.75	1007.83
	S.Ilario (B)	5.23	9.04	-4.37	13.95	9.57	919.40
	S.Ilario (C)	4.64	11.84	-6.53	17.48	10.94	1303.72
	S.Ilario (P)	4.28	10.57	-5.42	15.86	10.44	1218.26
	S.Ilario (S)	4.71	12.69	-7.27	18.54	11.27	1315.69
	Borgo A	1.71	4.07	1.91	5.79	7.69	576.44
	Borgo B	2.92	4.81	1.89	6.84	8.73	571.79
	Marradi	1.59	2.72	3.11	4.39	7.50	632.54
+2 °C -10 % 394 ppm	CH-Cha	4.58 (+0.29)	13.02 (-0.49)	-3.02 (+0.62)	20.58 (-0.70)	17.56 (-0.08)	884.33 (+3.00)
	AT-Neu	6.27 (+0.22)	11.39 (-1.18)	2.14 (+1.50)	15.44 (-1.54)	17.58 (-0.04)	610.87 (-22.92)
	IT-Tor	3.89 (+0.46)	6.44 (+0.90)	0.30 (+0.30)	8.65 (+1.19)	8.96 (+1.51)	545.05 (+41.30)
	S.Ilario (A)	3.98 (+0.10)	9.49 (-0.30)	-4.68 (+0.47)	14.52 (-0.38)	9.84 (+0.09)	1035.37 (+27.54)
	S.Ilario (B)	5.32 (+0.09)	8.85 (-0.19)	-3.95 (+0.42)	13.69 (-0.26)	9.74 (+0.17)	935.63 (+16.23)
	S.Ilario (C)	5.15 (+0.51)	11.85 (+0.01)	-6.22 (+0.31)	17.50 (+0.02)	11.28 (+0.34)	1353.18 (+49.46)
	S.Ilario (P)	4.11 (-0.17)	10.28 (-0.29)	-4.81 (+0.61)	15.50 (-0.36)	10.69 (+0.25)	1234.30 (+16.04)
	S.Ilario (S)	5.22 (+0.51)	12.61 (-0.08)	-6.86 (+0.41)	18.46 (-0.08)	11.59 (+0.32)	1369.66 (+53.97)
	Borgo A	2.09 (+0.38)	3.94 (-0.13)	2.75 (+0.84)	5.67 (-0.12)	8.42 (+0.73)	562.14 (-14.30)
	Borgo B	2.97 (+0.05)	3.95 (-0.86)	3.14 (+1.25)	5.74 (-1.10)	8.89 (+0.16)	554.42 (-17.37)
	Marradi	2.04 (+0.45)	3.11 (+0.39)	3.97 (+0.86)	4.92 (+0.53)	8.89 (+1.39)	610.32 (-22.22)
+2 °C -10 % 540.5 ppm	CH-Cha	4.85 (+0.56)	14.16 (+0.65)	-3.47 (+0.17)	22.29 (+1.01)	18.82 (+1.18)	880.04 (-1.29)
	AT-Neu	6.63 (+0.58)	12.26 (-0.31)	2.43 (+1.79)	16.58 (-0.40)	19.00 (+1.38)	610.31 (-23.48)
	IT-Tor	4.31 (+0.88)	7.26 (+1.72)	0.05 (+0.05)	9.71 (+2.25)	9.76 (+2.31)	542.09 (+38.34)
	S.Ilario (A)	4.39 (+0.51)	10.49 (+0.70)	-5.45 (-0.30)	15.82 (+0.92)	10.38 (+0.63)	1026.00 (+18.17)
	S.Ilario (B)	5.60 (+0.37)	9.54 (+0.50)	-4.48 (-0.11)	14.62 (+0.67)	10.14 (+0.57)	925.37 (+5.97)
	S.Ilario (C)	5.54 (+0.90)	12.98 (+1.14)	-7.12 (-0.59)	18.98 (+1.50)	11.87 (+0.93)	1346.31 (+42.59)
	S.Ilario (P)	4.72 (+0.44)	11.32 (+0.75)	-5.69 (-0.27)	16.86 (+1.00)	11.17 (+0.73)	1229.67 (+11.41)
	S.Ilario (S)	5.50 (+0.79)	13.80 (+1.11)	-7.75 (-0.48)	20.01 (+1.47)	12.26 (+0.99)	1367.56 (+51.87)
	Borgo A	2.36 (+0.65)	4.50 (+0.43)	2.58 (+0.67)	6.41 (+0.62)	8.98 (+1.29)	561.34 (-15.10)
	Borgo B	3.41 (+0.49)	4.60 (-0.21)	2.77 (+0.88)	6.59 (-0.25)	9.36 (+0.63)	555.15 (-16.64)
	Marradi	1.75 (+0.16)	2.83 (+0.11)	4.21 (+1.10)	4.59 (+0.20)	8.79 (+1.29)	607.62 (-24.92)

AGB = Above-ground biomass; NEE = Net Ecosystem Exchange; GPP= Gross Primary Production; RECO = Ecosystem respiration; ET = Evapotranspiration

%, AGB = -16.92 %) statistics among the Alpine sites. For the Mediterranean sites, best performances for LAI and AGB simulations were found at Marradi site (MAE = 45 g d.m. m^{-2} and 32 g d.m. m^{-2}; NRMSE = 35.94 % and 26.95 %, pBIAS = -22.71 % and -41.08 % for LAI and AGB, respectively).

Furthermore, the model satisfactorily simulated the water dynamics along the proposed climatic transect, from the Alps (IT-Tor, AT-Neu) to the inner region (Borgo; Fig. 4 and S5). At the Alpine sites, the simulated FTSW average trend for IT-Tor (2012–2018) and AT-Neu (2002–2006) reproduced the observations (r = 0.91; RMSE = 0.15, MAE = 0.13, NRMSE = 25.97 %, EF = 0.13 and CRM = 0.10, averaged over all data). Satisfactory performances of the FTSW were also obtained in Borgo (r = 0.95; RMSE = 0.13, MAE = 0.08, NRMSE = 13.25 %, EF = 0.91 and CRM = -0.02), although the dataset was limited to a single season data. On the other hand, the model showed poorer results in the simulation of evapotranspiration (ET mm; Table 3 and S2), on average for all sites in Alpine chain where observed data were available.

The carbon litter simulations ranged from 2.48 Mg C ha^{-1} y^{-1} (Borgo A) to 14.13 Mg C ha^{-1} y^{-1} (AT-Neu). This daily fraction, identified in spin up process, was used as input to the RothC model. In detail, the model spin-up showed a higher percentage distributed in the humified pool and a lower percentage in the inert pool in sites located in Alpine chain compared to the Mediterranean ones (Table S4).

The simulations of water and carbon fluxes were in good agreement with the observations, as shown in Table S3 and in Figs. 5 and S7–8. Sites where eddy covariance data were available showed a different observed net carbon uptake, with CH-Cha and IT-Tor evidencing negative annual NEE values (-2.88 ± 1.99 and -0.37 ± 0.63 Mg C ha^{-1} on average, respectively), while AT-Neu showed a net carbon emission (NEE = +3.74 ± 1.73 Mg C ha^{-1} on average). For these sites, GRASSVISTOCK model simulated annual NEE values of -2.99 ± 1.91 Mg C ha^{-1}, +0.64 ± 1.93 Mg C ha^{-1} and -0.002 ± 0.82 Mg C ha^{-1} on average for CH-Cha, AT-Neu and IT-Tor sites, respectively. Similar to NEE, the GRASSVISTOCK model was able to reproduce GPP, RECO and ET at CH-Cha, AT-Neu and IT-Tor (Table S3). The statistics of the correlation between observed and simulated annual NEE, GPP, RECO and ET values are shown in Fig. 5 for all sites, while the performances between observed and simulated data of daily and 10-days trends are shown in Figs. S7–8. The model showed a better performance for daily simulated NEE in IT-Tor (r = 0.61; RMSE = 0.02 Mg C ha^{-1}) compared to the other two sites (CH-Cha: r = 0.35; RMSE = 0.04 Mg C ha^{-1}; AT-Neu: r = 0.27; RMSE = 0.04 Mg C ha^{-1}). This trend is also confirmed for GPP and RECO, with IT-Tor showing the highest performances (GPP: r = 0.85; RMSE = 0.02 Mg C ha^{-1}; RECO: r = 0.65; RMSE = 0.02 Mg C ha^{-1}). On the other hand, ET showed the highest r value in CH-Cha (0.80) and the lowest RMSE value in IT-Tor (1.37 mm). The other statistics related to the fluxes are reported in Table S2.

3.2. Model application

The calibrated model was applied on modified climate datasets, representing the increase in temperature, the decrease in precipitation and a CO_2 enriched environment expected in the future, to outline possible consequences of climate change on the grassland ecosystem performance under warmer and drier conditions (Fig. 6).

In the present period, the sites experiencing mild temperature and favourable precipitation regime (CH-Cha) or supported by irrigation (S. Ilario), exhibited negative NEE values (-3.64 ± 1 and -5.75 ± 1.15 Mg C ha^{-1}, respectively), with the only exception of AT-Neu, characterised by positive NEE value (+0.64 ± 1.93 Mg C ha^{-1}). The NEE results for CH-Cha and S. Ilario were derived from higher GPP compared to RECO values while higher RECO compared to GPP was found in AT-Neu (Table 4). Conversely, in sites characterised by shorter (IT-Tor) or drier (Borgo A and B and Marradi) growing seasons, the balance between GPP and RECO resulted in neutral (-0.002 ± 0.82 Mg C ha^{-1}, IT-Tor) or positive NEE (2.30±1.04 Mg C ha^{-1} on average for Borgo A, B and Marradi; Table 4).

The combination of increasing temperature, decreasing precipitation and higher CO_2 concentration resulted, in an increase of the peak AGB (+0.58 Mg d.m. ha^{-1}) and total AGB (+0.60 Mg d.m. ha^{-1}), averaged over all study cases and compared to the present period indicating the positive effect of a CO_2 enriched environment (average of all sites). On the other hand, the scenario with increasing temperature, decreasing precipitation and reference CO_2 showed a general increase in the AGB peak and a decrease in the total AGB (peak AGB: +0.26 and total AGB: -0.20 Mg d.m. ha^{-1}, averaged of all sites), although this positive effect is less evident when compared to the previous scenario. Concerning the carbon fluxes, the scenario with elevated atmospheric CO_2 concentration showed a general increase in GPP with respect to the present period (+0.82 Mg C ha^{-1}, averaged over all study cases). However, the higher impact of climate change on RECO (+1.08 Mg C ha^{-1}, averaged over all study cases) resulted in higher net CO_2 emissions than in the present period (NEE: +0.27 Mg C ha^{-1}, averaged over all study cases). The S. Ilario site, where irrigation was applied in all farms, represented an exception where the average NEE decreased by -0.35 Mg C ha^{-1} (net carbon uptake increased), comparing the present period with the atmospheric CO_2 enriched scenario.

In the enriched CO_2 scenario, the increase in CO_2 concentration from 394 to 540.5 ppm smoothed the impact of a warmer climate on ET by reducing its increase from +11.89 mm to +7.90 mm (average among all study cases).

Carbon fluxes showed two opposite trends at seasonal scale: in springtime, carbon uptake generally increased in all sites while this trend was reversed in summer. In the first part of the season, when soil water conditions were not yet limiting (Fig. S9), the earlier and higher photosynthetic activity led to higher GPP compared to the present period (+0.90 Mg C ha^{-1} during January-April period). This positive effect on GPP was not fully counterbalanced by a proportional increase in RECO (+0.47 Mg C ha^{-1}), which ultimately led to an increase in carbon uptake in this part of the season (NEE: -0.43 Mg C ha^{-1} during January-April period) with respect to the present period and across all sites and study cases. This trend was reversed in May-September, where drier and warmer conditions reduced GPP (-0.10 Mg C ha^{-1}) and increased RECO (+0.40 Mg C ha^{-1}), hence determining a shift towards an increase in NEE (+0.50 Mg C ha^{-1}) in the CO_2 enriched scenario with respect to the present period (Fig. S9). The NEE increase was reduced in S. Ilario because of the applied irrigation (+0.13 Mg C ha^{-1}). There were negligible variations of carbon and water fluxes in winter time, especially in sites characterised by permanent snow cover (e.g. November - April IT-Tor, NEE: from -0.002 Mg C ha^{-1} (min) to 0.04 Mg C ha^{-1} (max) over the present period). Increased CO_2 concentration mitigated the negative effects of climate change. Over the growing season, when the effect of CO_2 on ε_{maxCO2} and TEC_{CO2} was removed in the simulation, NEE increased by +0.43 Mg C ha^{-1} in all sites as compared to the simulation including CO_2 concentration. On a seasonal scale, the positive trend in carbon uptake observed in January-April (NEE: -0.43 Mg C ha^{-1}) was slightly downsized when the effect of CO_2 was removed (NEE: -0.26 Mg C ha^{-1}) with respect to the present and in the same period. In summer, by removing the CO_2 effect, NEE increased by +0.28 Mg C ha^{-1} with respect to the simulation under higher CO_2 concentration.

4. Discussion

4.1. Model implementation, calibration and evaluation

The results of this study showed that the GRASSVISTOCK model was able to reproduce the grassland growth dynamics and the ecosystem fluxes in sites characterised by contrasting climates and management practices (Figs. 3-5). The presented model is based on the architecture presented in Bellini et al. (2013b), but broadens its applicability and achievable outputs. In contrast to the approach of Bellini et al. (2023b), where the grass development and growth dynamics were simulated

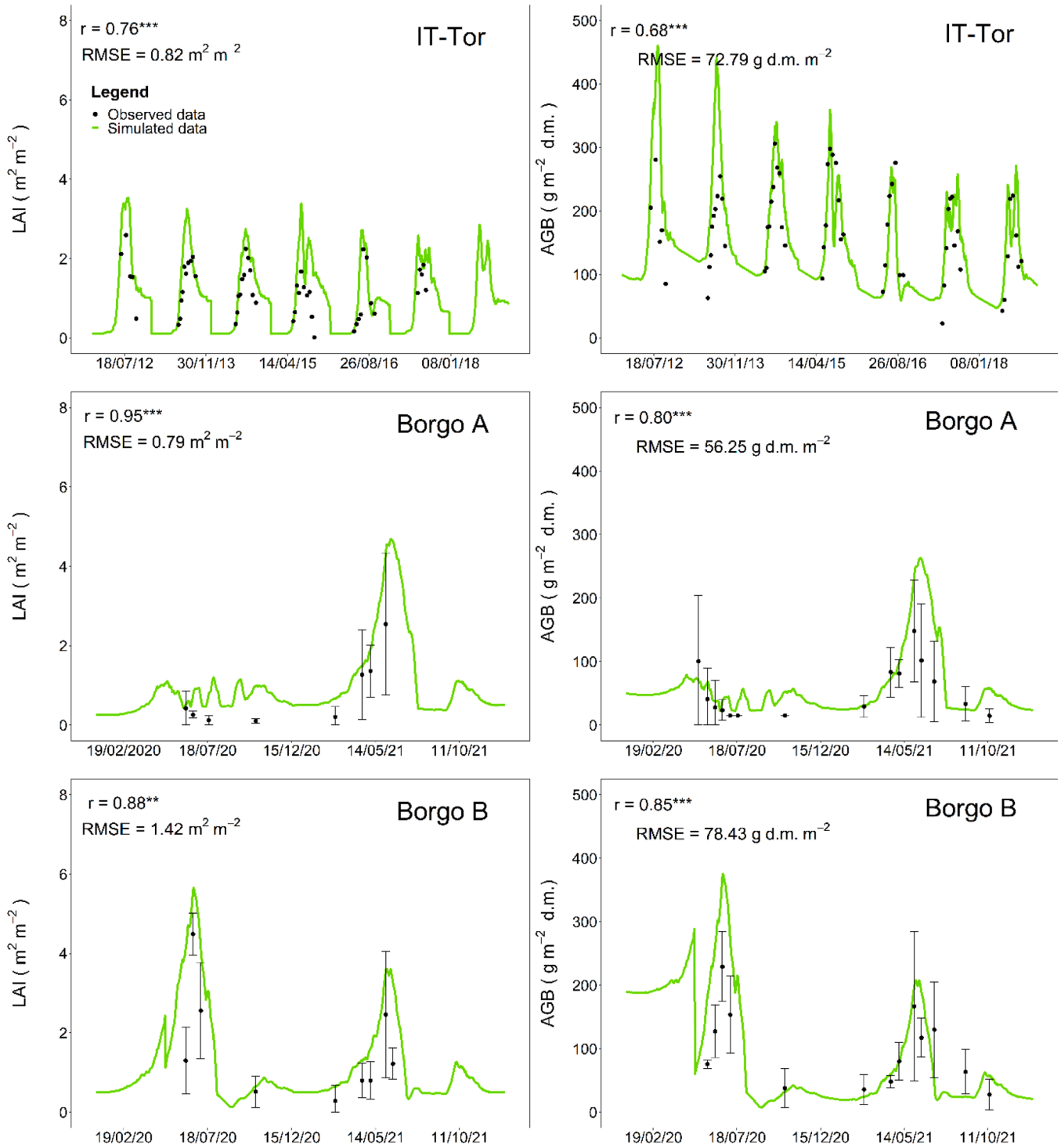

Fig. 3. Comparison and performance statistics between observed and simulated LAI and AGB data in IT-Tor (unmanaged Alpine grassland, 2012–2018) and in Borgo (managed Mediterranean pasture 2020–2021; Borgo A and B refer to two different managements as reported in Table 1). p-value: (ns, not significant; •, $p<0.05$; **, $p<0.01$; ***, $p<0.001$).

based on a diagnostic NDVI-derived LAI approach, in this new version a prognostic strategy for simulating LAI dynamics was proposed to increase the model applicability. Considering the reliability of the diagnostic approach in estimating LAI as a driver of biomass accumulation in grasslands (Bellini et al., 2023b; He and Mostovoy, 2019), the LAI and AGB outputs of the current configuration (modelled LAI) were first compared with the results derived by the model forced with NDVI-derived LAI strategy. The NDVI-derived LAI approach (Bellini et al., 2023b), in which LAI is estimated from satellite observations of grasslands, resulted in higher performance of LAI and AGB simulations compared to the alternative LAI prognostic model (Fig. S4). Nevertheless, although the prognostic approach may appear to be less accurate, it is driven exclusively by the simulation of physiological processes based on meteorological inputs. This second alternative enables the prediction of the dynamic of both variables without the need for external data to force simulation, thus allowing to account for daily grass growth and

ecosystem fluxes under present and future climates. The prognostic approach demonstrated acceptable performance in simulating grass growth dynamics across the proposed climatic transects, taking into account potential perturbing factors such as mowing, grazing and irrigation. The model's simple architecture, comprising a reduced number of modelled processes and parameters to be calibrated, entailed the inclusion of plant parameters pertaining to the leaf area development and those limiting photosynthetic efficiency in the calibration process. The remaining parameters were defined by literature and assumed as constant during the simulations (Table 2). The calculation of GPP, which is dependent on light interception and maximum potential radiation use efficiency (ε_{maxref}) as reduced by thermal and water stresses, represents the core of the simulation model. While ε_{maxref} was assumed as constant for all sites (1.65 g C MJ^{-1}; Heinsch et al., 2003; Maselli et al., 2013), a reliable simulation of the gross assimilation rate required a local parametrization of coefficients regulating LAI development (e.g. leaf lifespan, $Leaf_{Life}$), as well as the effect of thermal stress on photosynthesis (GT_{min} and GT_{opt}) during the season. $Leaf_{Life}$ varied across the sites ranging from 163.92 °C days (IT-Tor) to 500 °C days (S.Ilario). This likely reflects the influence of diverse factors, including the phenology of different vegetation composition, environmental conditions and agro-management practices at each site (Reich et al., 1998; Karatassiou and Noitsakis, 2010; Schleip et al., 2013). As an example, Reich et al. (1998) showed that distinct leaf lifespan and specific leaf area can be observed for different grass species belonging to the same functional group across different ecosystem types (i.e. from alpine tundra/subalpine to tropical rainforest).

The local calibration of GT_{min} and GT_{opt} showed that the relevant values were positively correlated to mean annual air temperature across the considered regions (Fig. S2). This relationship was in accordance with the results found by Bellini et al. (2023b) and Maselli et al. (2013) in a modelling approach, which showed that warmer climates exhibit higher temperature thresholds defining photosynthetic limits (Berry and Bjorkman, 1980; Chang et al., 2021b; Hikosaka et al., 2006). The only exception to this trend was observed at IT-Tor, which, despite being the coldest site, exhibited a relatively high GT_{opt} (Fig. S2). This particular behavior may be related to the specific climatic conditions of IT-Tor (Table 1), which are characterised by a prolonged winter period of snow cover (~ 6 months, on average over the study period). This leads to a shorter vegetative growing season and a relatively higher minimum temperature for optimal grass growth (GT_{opt}) compared to AT-Neu and CH-Cha (AT-Neu snow cover: ~2.5 months, no continuous CH-Cha snow cover: ~1 month on average over the study period). It is noteworthy that the use of these empirical relationships (Fig. S2), simplifies the parameterisation of T_{cor} in areas where it has not yet been tested, employing the average temperature of the location as driving parameter.

The GRASSVISTOCK model provided an acceptable estimation of AGB (Fig. 3), which was calculated as the difference between the GPP and plant respiration. This accounts for the autotrophic component of ecosystem respiration (Marconi et al., 2017; Wang et al., 2019a). Despite its intrinsic limitations (Thornley and Cannell, 2000: Collalti et al., 2020), this paradigm is still adopted for modelling plant respiration, with satisfactory results for grassland (Amato and Gimenez, 2022). It was considered particularly suitable for the proposed parsimonious modelling scheme. This approach revealed that temperature exerts a direct influence on respiration activity, as it has been corroborated by other studies (Amthor, 1984; Szaniawski and Kielkiewicz, 1982). Indeed, the results of the calibration of the maintenance respiration coefficient (*km*) demonstrated an increase in this parameter accordance with rising temperatures (Fig. S10). With this regard, although the results indicated that *km* is species- and site-specific, the relationship shown in Fig. S10 may facilitate the model applicability in new areas.

The parametrization of an individual species or variety is a feature of crop models that undoubtedly shows positive aspects in terms of the simplification of simulated processes, without taking into account the growth dynamics of a multi-species system. This extreme simplification restricts the model applicability to numerous aspects, including the enhancement of the agronomic management and the evaluation of the impact of climate change on plant growth (Movedi et al., 2019). However, very complex modelling approaches may increase simulation uncertainty if not properly calibrated and validated (Soussana et al., 2012; Movedi et al., 2024). In light of the difficulty of obtaining observed data of a wide floristic composition, the simplified approach proposed in this study can be considered an acceptable compromise in terms of the performance obtained for flux simulation (Section 3.2). In addition, the overall consistency of the model in estimating growth processes and the associated transpiration is demonstrated by its ability to reproduce soil water balance, as evidenced by the results for IT-Tor, AT-Neu and Borgo sites (Fig. 4). Considering that water stress plays a major main role on grassland growth and forage quality (Habermann et al., 2019; Mastalerczuk and Borawska-Jarmułowicz, 2021), a satisfactory estimation of the soil water content availability is important for modelling grassland growth (Bellini et al., 2023b; Sándor et al., 2017). Once more, these findings were obtained by considering the parameters driving potential transpiration (TEC_{ref}) and the effect of water stress on it as constants, thereby representing an average grassland comprising diverse species. This assumption aligns with the original VISTOCK model (Bellini et al., 2023b) by allowing model application in different climatic and environmental contexts. For example, moving from the wet conditions of IT-Tor and AT-Neu sites, which are favoured by high precipitation and lower temperatures, to the severe water stress typical of a Mediterranean summer (e.g. Borgo; Fig. 4).

In all study cases, the water stress was slightly underestimated during the summer periods (Fig. 4). This trend may be attributed to several factors. Firstly, SWC was expressed as FTSW, which is used as scalar to reduce photosynthesis and transpiration. Its limits, 0 (wilting point) and 1 (field capacity), were determined by the series of observed data, with 0 corresponding to the lowest SWC found and 1 to the highest one. It is evident that this approximation can generate a level of uncertainty regarding the water that can potentially be contained in the soil layer. This may result in an overestimation of the water stress in case the lower limit of FTSW is fixed for a relatively too high SWC. Nevertheless, a certain degree of overlap is observed between the variability parameter of the curves, indicating that the simulated and observed FTSW exhibit a similar seasonal pattern. This is corroborated by the highly significant value of the Pearson's correlation coefficient found for Borgo (0.95) and IT-Tor (0.88), $p<0.001$. Moreover, the approach used was based on the identification of two single soil layers, wherein precipitation and irrigation represented the inputs, while evapotranspiration represented the main output of the water balance (Bellini et al., 2023b). Thus, the model does not take into account phenomena such as capillary rise and runoff that may affect the water balance during the growing season (Soltani and Sinclair, 2012). Notwithstanding the level of uncertainty, the model still showed an overall consistency in the estimation of the effect of water stress on the accumulation of above-ground biomass and fluxes, making the bias found acceptable. The GRASSVISTOCK model was able to capture the seasonal grass growth trend of the different sites, as generally characterised by a rapid increase in biomass early in the season followed by a phase of progressive senescence. This result is further supported by simulations in sites where management practices were applied throughout the season (e.g. AT-Neu, Borgo and Marradi) and the model identified grass recovery after mowing or grazing. However, the performance between the observed and simulated AGB values was found to be lower than those reported in other studies (Bellini et al., 2023a; Petersen et al., 2021; Pulina et al., 2018), where the use of a more advanced model (i.e. PaSim) showed better performances in estimating AGB (Table S2). As previously described, the advantages generated by the use of a simplified modelling approach in terms of executability, adaptability, and general applicability may be associated with lower estimation accuracy of some processes that a more advanced and complex modelling solution is able to account for.

Differently from AGB, BGB observed data were not available for

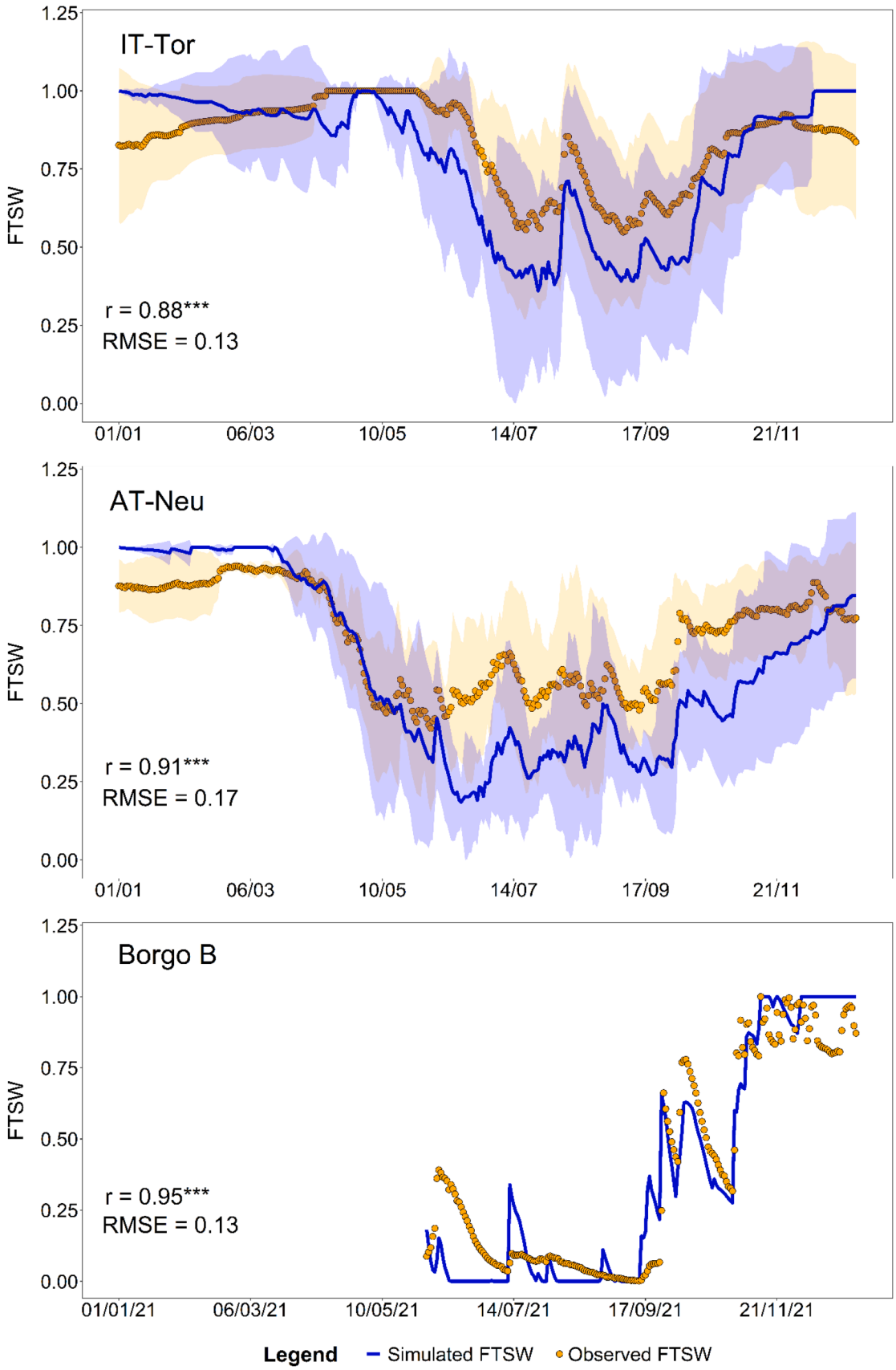

Fig. 4. Comparison between observed (orange) and simulated (blue) FTSW data in IT-Tor, AT-Neu and Borgo B. The average FTSW trends and the standard deviations are displayed for IT-Tor and AT-Neu during the periods 2012–2018 and 2002–2006, respectively. The FTSW trend from June to December 2021 only is reported for Borgo B, due to the lack of further observations. The statistics were calculated on the average trends of FTSW data in IT-Tor and AT-Neu and on the FTSW data from 2021 in Borgo. p-value: (ns, not significant; •, $p<0.05$; **, $p<0.01$; ***, $p<0.001$).

model validation. Consequently, the senescence rate was approximated using a fixed root turnover ratio (0.3 year^{-1}, as reported by Wang et al., 2019b; Garcia-Pausas et al., 2011). In the absence of data, some considerations can be drawn based on the data reported in the literature. In general, the standing total BGB (living and dead roots) is higher in sites with higher AGB (data not shown). This trend reflects what observed by Yang et al. (2018), who found a positive correlation between BGB and AGB. The estimated BGB of perennial forages in Europe is reported by Bolinder et al. (2012) to be approximately 7.9 Mg ha^{-1}, on average. However, the high degree of variability, from 1.1 to 47.3 Mg ha^{-1}, makes difficult to draw a conclusion on the accuracy of simulation. Amato and Gimenez (2022) found a smaller variability range for grasslands across different regions, but their analysis further suggests that steady BGB biomass is higher in cooler climates. To illustrate, the total BGB of Charleville (Australia; Christie, 2014), with an average mean annual temperature (MAT) of 21 °C, reached from ~1.07 Mg ha^{-1} for C3 to ~4.05 Mg ha^{-1} for C4 species, while shifting to a colder climate (e.g. Montecillo, Mexico, MAT = 15.6 °C; Garcia-Moya, 2015), BGB yielded in average ~11.7 Mg ha^{-1}. Even cooler sites, like Dickinson (USA, MAT = 6 °C, Whitman and Lauenroth, 2014) and Shortandy (Kazakhstan, MAT = 2.3 °C, Gilmanov, 2015) yielded a total BGB is up to ~30 Mg ha^{-1} for grazed grasslands in the first case and up to ~40 Mg ha^{-1} in the second case that is in the range of what is simulated for colder and managed sites of CH-Cha and AT-Neu. The S. Ilario site, which is characterised by high AGB production and the application of irrigation management, exhibited similar BGB values (data not shown). In particular, a reasonable simulation of AGB and BGB accumulation suggests that the GRASSVISTOCK model can reproduce the amount of total annual plant carbon litter, i.e. the yearly accumulated senesced matter from AGB and BGB in CH-Cha and AT-Neu (11.62 ± 3.08 Mg C

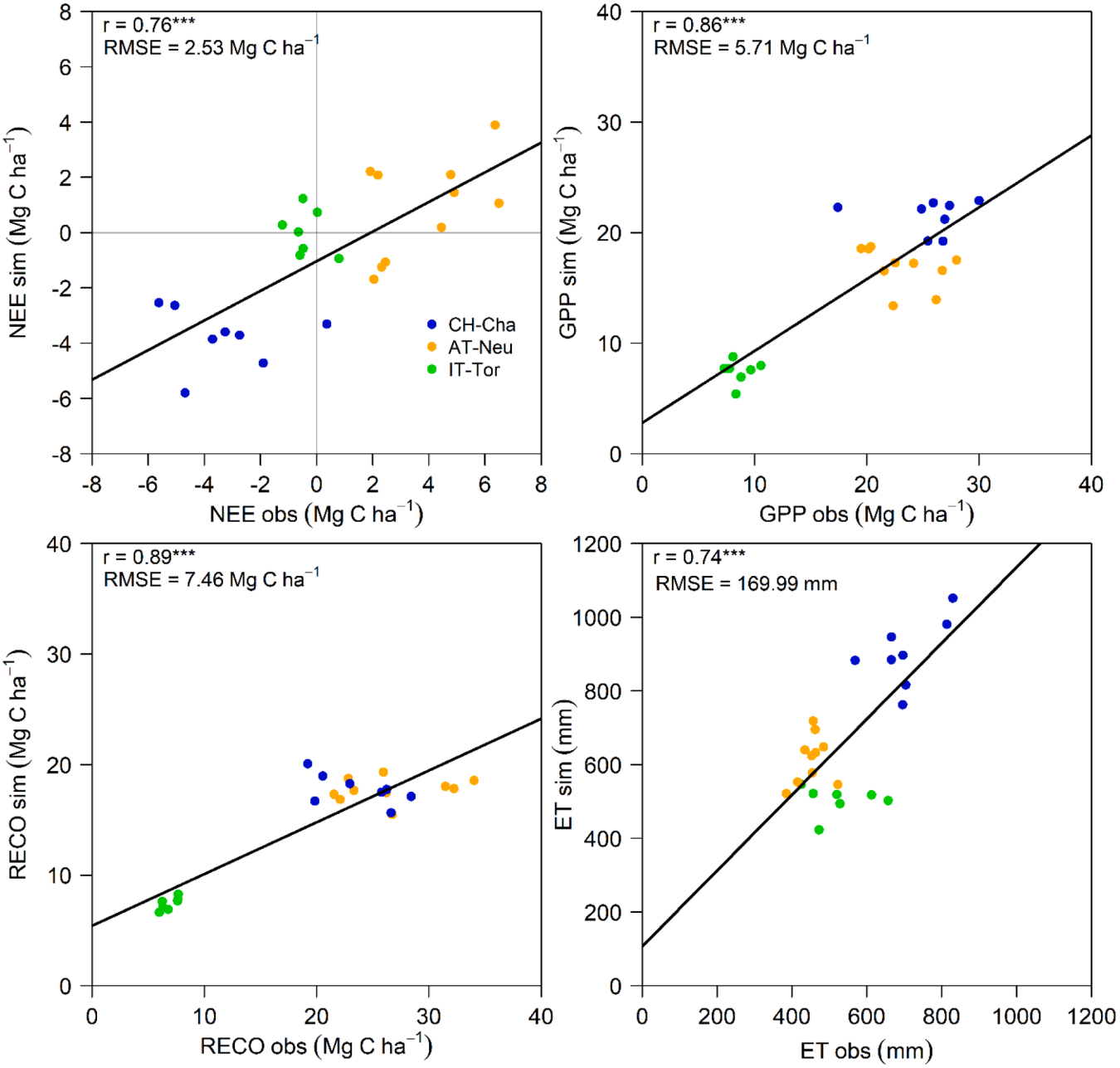

Fig. 5. Correlations between annual observed (obs) and simulated (sim) data of NEE (Mg C ha^{-1}), GPP (Mg C ha^{-1}), RECO (Mg C ha^{-1}) and ET (mm) for CH-Cha, AT-Neu and IT-Tor sites located in Alpine chain. The years in which some data were removed (i.e. AT-Neu 2002, CH-Cha 2005 and 2009) were excluded. p-value: (ns, not significant; •, p<0.05; **, p <0.01; ***, p<0.001).

ha^{-1} y^{-1}, on average). This is in line with the value reported by De Bruijn et al. (2012) for a similar environment and management system (i.e. managed grassland in the Swiss Alps) which accounts for an annual contribution of 13.40 Mg C ha^{-1} y^{-1} (average among intensive and extensive management experiments).

In this context, the RothC module was selected for routinely simulating the SOC turnover and the soil heterotrophic respiration, in accordance to the outputs provided by GRASSVISTOCK. Differently to other soil carbon models (e.g. CENTURY), the RothC model exclusively estimates the carbon cycle without accounting for other elements (e.g. nitrogen, phosphorus and sulfur), which may limit the model capability at describing a complete analysis of biogeochemical cycles. However, the restricted number of inputs required for RothC simulations, which allows for a wider range of spatial-scale applications (Morais et al., 2019), is consistent with the ratio used in the development of GRASSVISTOCK. As previously described, GRASSVISTOCK aims to limit model input data and maximize its applicability in different environmental and climatic contexts, thereby providing a comprehensive overview of the ecosystem carbon balance.

4.2. *Ecosystem fluxes and model application*

The model demonstrated satisfactory performance in simulating grassland carbon fluxes in Alpine sites where eddy covariance datasets were available (Figs. 5 and S8). In general, GRASSVISTOCK underestimated GPP and RECO in all study sites, a finding that is consistent with similar studies (Sándor et al., 2020; Forster et al., 2022). This behaviour may be attributed to the fact that, in the present study, model

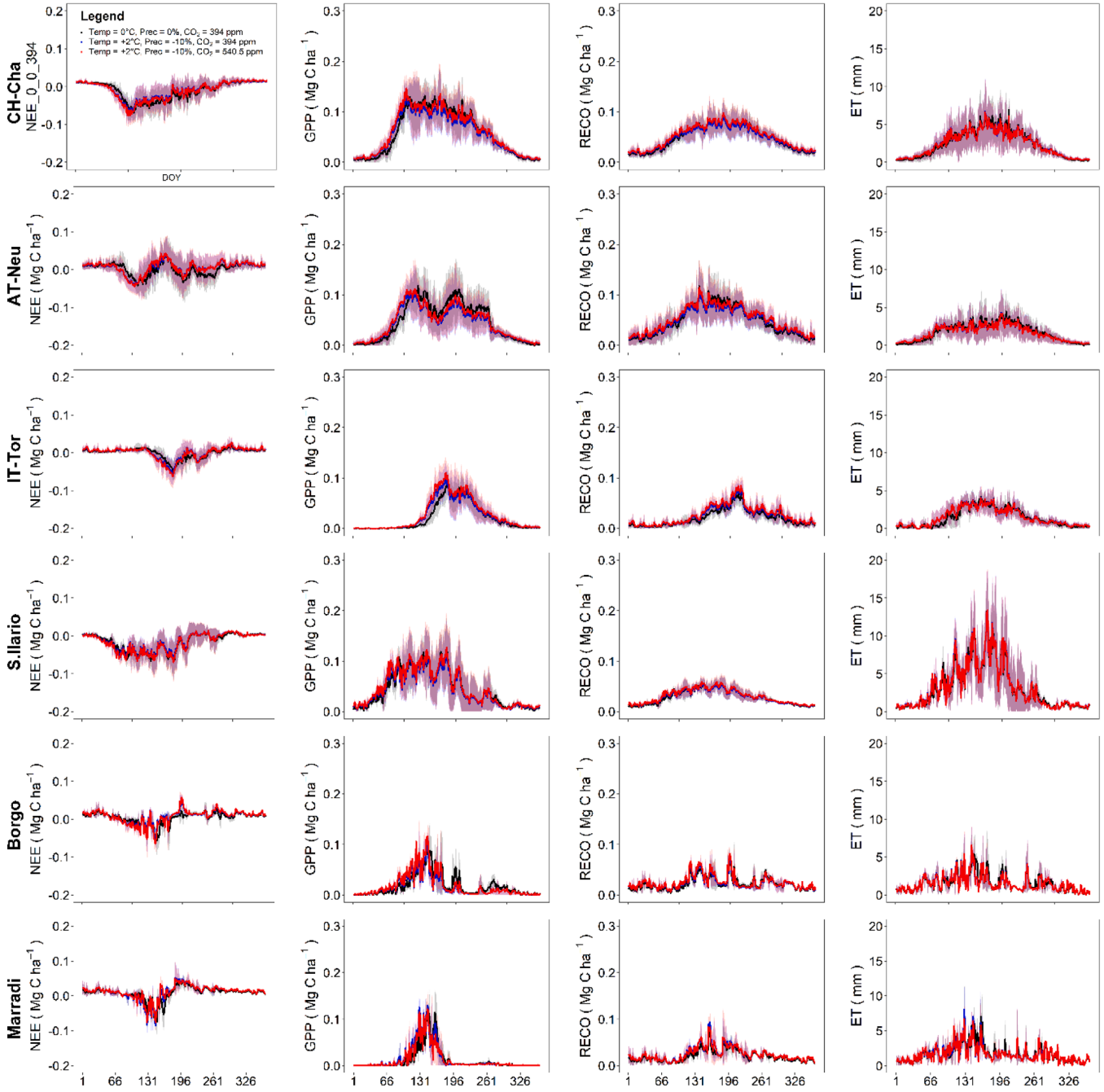

Fig. 6. Seasonal average trend of NEE (Mg C ha^{-1}), GPP (Mg C ha^{-1}), RECO (Mg C ha^{-1}) and ET (mm) of the present (black line - 0 °C, 0 %, 394 ppm) and future climates (blue line - +2 °C, -10 %, 394 ppm; red line - +2 °C, -10 %, 540.5 ppm).

calibration was performed on NEE, which ultimately represents the only observed data from eddy covariance. In contrast, GPP and RECO are derived using partitioning algorithms (e.g. Nighttime vs Daytime; Pastorello et al., 2020; Lasslop et al. 2010, Reichstein et al., 2005). This implies that an ad-hoc calibration on GPP and/or RECO, in place of the observed NEE from eddy covariance, may result in an overestimation of the latter (see Section 2.4).

The results obtained in this study align with those of previous modelling exercises (Sándor et al., 2020; Forster et al., 2022), in which different models were initially calibrated against vegetation, soil and carbon fluxes data in grasslands and croplands. In this context, an ensemble of grassland models (e.g. APSIM-GRAZPLAN, APSIM-SoilWater, DairyMod, PaSim, etc.) was used for simulating NEE, GPP and RECO in two grasslands of France and the United Kingdom. The results of the median of the simulation obtained by Sándor et al. (2020) in Laqueielle grassland of France were in agreement in terms of correlation coefficient (r) with the results of this study obtained across Alpine sites (NEE: 0.55 vs 0.45, GPP: 0.79 vs 0.74; RECO: 0.75 vs 0.61 for Sándor et al., 2020 and GRASSVISTOCK, respectively). On the other hand, the Nash-Sutcliffe modeling efficiency (EF) of Sándor et al. (2020) ranges from -0.65 to 0.62 for GPP, from -4.26 to 0.45 for NEE and from -1.52 to 0.52 for RECO, when observed and simulated values were compared for grassland sites and different calibration stages. These results were lower compared to those obtained in our study, where EF ranges from 0.41 to 0.44 for GPP, from -0.80 to 0.25 for NEE and from 0.10 to 0.21 for RECO. In Forster et al. (2022), the RMSE values of NEE, GPP and RECO obtained using DNDC model in a Finnish grassland were found in agreement with the RMSE calculated in this study across the Alpine sites (NEE: 0.027 vs 0.03 Mg C ha^{-1}, GPP: 0.0351 vs 0.04 Mg C ha^{-1}, RECO: 0.0142 vs 0.04 Mg C ha^{-1} for DNDC and GRASSVISTOCK models, respectively). In the same study, the pBIAS was found -20.7 % for GPP, -14.2 % for NEE and -22.8 % for RECO which was in agreement to our results of GPP -9.74 % (min: -25.86 %; max: 15.84 %) and RECO -18.45 % (min: -33.16 %; max: 4.90 %) and higher for NEE -59.51 % (min: -99.38 %; max: 3.89 %).

Despite the relevant differences in species composition, climate, and agronomic management (Table 1), the results of model calibration for NEE showed a satisfactory agreement with observations in CH-Cha AT-Neu and IT-Tor, thereby establishing the viability of further application of the tool to reproduce grassland dynamics in different environmental conditions (Figs. 5 and S7–8). In Mediterranean sites, where flux observations were not available, the GRASSVISTOCK model was firstly calibrated against observed LAI and AGB variables, and then used for simulating carbon fluxes. Although the model was not calibrated using the variable NEE at these sites, we considered that the model calibration on LAI and AGB variables and a proper simulation on water dynamics may be a satisfactory condition for carbon cycle estimation. This is also in line with the tests performed at the IT-Tor site, where no significant differences between the calibrations performed with or without the use of NEE were found (Fig. S1 and Results section).

The application of the model under higher temperature and lower precipitation evidenced an average increase of the AGB peak in all study cases analyzed, irrespective of CO_2 atmospheric concentration (Fig. 6 and Table 4) and an associated advancement of the start of vegetative growth (Fig. S9) as already observed (Bellini et al., 2022) and simulated (Petersen et al., 2021) across Europe in response to climate change. In contrast, during summer, the combined effect of elevated temperatures and stressful soil moisture conditions resulted in a net reduction in total AGB, particularly when these conditions were not counterbalanced by the positive impact of the enriched atmospheric CO_2 concentration on plant growth. With regard to fluxes, a decrease in carbon uptake capacity (i.e. NEE increase) is shown in the scenario characterized by the reference atmospheric CO_2 concentration while it is improved (i.e. NEE decrease) under enriched CO_2 concentration due to the positive impact of CO_2 on εmax_{CO2} and TEC_{CO2}. In accordance with the observed trend in AGB, an increase of carbon uptake capacity was shown in the first part of the season where the higher temperature and non-stressful soil water conditions determined a positive impact on GPP, which is then converted in NPP and AGB (Fig. S9). In summer, the combined effect of higher temperature and lower soil water content determined an average higher increase of RECO compared to GPP which reduce the carbon uptake capacity (i.e. NEE increase). The enriched CO_2 scenario was shown to reduce this gap with a consequent limited downward trend of NEE, as similarly reported in other studies on grasslands where the elevated atmospheric CO_2 concentrations are expected to mitigate the impact of high temperature and drought on net ecosystem exchange (Franks et al., 2013; Roy et al., 2016).

This results in an increase in the discrepancy between the potential carrying capacity that could be achieved during the spring and summer periods and the actual carrying capacity that cannot support the same number of animals due to a significant decline in AGB production. This could influence farm area management strategies by seeking an equilibrium between the area dedicated to grazing and that dedicated to fodder stock production, with the objective of supporting the higher load that can be assumed from the expected increase in the spring period. The results obtained in S.Ilario, where higher CO_2 concentration and application of summer irrigation determined higher AGB and lower NEE values (Table 4), indicated that irrigation practice in future climates may even enhance the capability of grasslands for carbon fluxes while increasing the relevant carrying capacity (Ryan et al., 2017; Doughty et al., 2018; Brilli et al., 2019, 2023). However, the use of water resources should be carefully considered in the view of its limited supply, the high costs and the extra-agriculture uses.

5. Conclusions

The GRASSVISTOCK model was able to simulate the LAI and AGB trends under different agro-management conditions (e.g. mowing, grazing and irrigation), to reproduce the FTSW dynamics under extremely different soil water conditions in summer (e.g. IT-Tor vs Borgo) and to satisfactorily simulate the ecosystem fluxes (NEE, GPP, RECO and ET), which represents a key point in order to support farmers' decisions during the optimization of farm management. Furthermore, the GRASSVISTOCK model application under present and future climates (+2 °C, temperature; -10 % precipitation; 394 or 540.5 ppm), indicates a general decrease in carbon uptake across all sites. This expected to provide useful information regarding the future sustainability and mitigation potential of Alpine and Mediterranean grasslands. Despite the positive impact of a CO_2 enriched environment, which partially counterbalances the negative effect of increasing temperature and decreasing precipitation on carbon uptake, the results of this study showed that climate change mitigation in grasslands will be strongly limited if no *ad-hoc* adaptation strategies were adopted (e.g. positive impact of applied irrigation in S.Ilario).

In light of the aforementioned findings, the simplified methodology proposed with GRASSVISTOCK model moves a step forward to describe carbon and water flux dynamics in European agro-pastoral-ecosystems, with the purpose to investigate the future sustainability of these systems under the projected climate scenarios and different managements. Future works should concentrate on the implementation of new modelling approaches, including the introduction of new modules for simulating soil and plant nitrogen dynamics and mixed grass and shrub/tree systems, as well as improvements to the estimation of grazing and its contribution to carbon dynamics. These developments will enhance the estimation of biogeochemical cycles and the assessment of the climate mitigation potential in grasslands.

Software availability

The current model version can be made available to end users upon reasonable request to the corresponding author.

CRediT authorship contribution statement

L. Leolini: Writing – review & editing, Writing – original draft, Validation, Software, Methodology, Investigation, Conceptualization. **S. Costafreda-Aumedes:** Writing – review & editing, Software, Conceptualization. **L. Brilli:** Writing – review & editing, Investigation, Writing – review & editing, Validation, Methodology. **M. Galvagno:** Writing – review & editing, Validation, Resources. **M. Bindi:** Writing – review & editing, Supervision. **G. Argenti:** Writing – review & editing, Investigation. **D. Cammarano:** Methodology, Writing – review & editing, Validation, Resources. **E. Bellini:** Writing – review & editing, Investigation. **C. Dibari:** Writing – review & editing, Investigation. **G. Wohlfahrt:** Writing – review & editing, Validation, Resources. **I. Feigenwinter:** Writing – review & editing, Validation, Resources. **A. Dal Prà:** Writing – review & editing, Resources, Investigation. **D. Dalmonech:** Writing – review & editing, Validation, Methodology. **A. Collalti:** Writing – review & editing, Investigation. **E. Cremonese:** Writing – review & editing, Resources. **G. Filippa:** Investigation. **N. Staglianò:** Writing – review & editing, Investigation. **M. Moriondo:** Writing – review & editing, Supervision, Methodology, Conceptualization.

Declaration of competing interest

The authors declare that they have no known competing financial interests or personal relationships that could have appeared to influence the work reported in this paper.

Acknowledgments

The publication was made by L.L. with a research contract co-funded by the European Union - PON Research and Innovation 2014–2020 in accordance with Article 24, paragraph 3a), of Law No. 240 of December 30, 2010, as amended and Ministerial Decree No. 1062 of August 10, 2021. We thank ICOS CP for providing the facilities on fluxes elaborated products for IT-Tor site. D.D. and A.C. acknowledge the project funded under the National Recovery and Resilience Plan (NRRP), Mission 4 Component 2 Investment 1.4 - Call for tender No. 3138 16 December 2021, rectified by Decree n.3175 of 18 December 2021 of Italian Ministry of University and Research funded by the European Union – NextGenerationEU under award Number: Project code CN_00000033, Concession Decree No. 1034 of 17 June 2022 adopted by the Italian Ministry of University and Research, CUP B83C22002930006, Project title “National Biodiversity Future Centre - NBFC”.

A.C. was supported by PRIN 2020 "Unraveling interactions between WATER and carbon cycles during drought and the impact on water resources and forest and grassland ecosySTEMs in the Mediterranean climate" (WATERSTEM, project number 20202WF530)’ and Multi-scale observations to predict Forest response to pollution and climate change” (MULTIFOR, project number 2020E52THS). I.F. was supported by the Swiss National Science Foundation (SNSF) in the project ICOS-CH phase 3 (20FI20_198227). SC-A and MB acknowledge the EU - Next Generation EU Mission 4 “Education and Research” - Component 2: “From research to business” - Investment 3.1: “Fund for the realisation of an integrated system of research and innovation infrastructures” - Project IR0000032 – ITINERIS - Italian Integrated Environmental Research Infrastructures System - CUP B53C22002150006.

Supplementary materials

Supplementary material associated with this article can be found, in the online version, at doi:10.1016/j.agrformet.2025.110486.

Data availability

The authors do not have permission to share data.

References

Amato, M.T., Giménez, D., 2022. Quantifying root turnover in grasslands from biomass dynamics: application of the growth-maintenance respiration paradigm and re-analysis of historical data. Ecol. Model. 467, 109940. https://doi.org/10.1016/j.ecolmodel.2022.109940.

Amthor, J.S., 1984. The role of maintenance respiration in plant growth. Plant Cell Environ. 7, 561–569. https://doi.org/10.1111/1365-3040.ep11591833.

Andren, O., Katterer, T., 1997. ICBM: the introductory carbon balance model for exploration of soil carbon balances. Ecol. Appl. 7, 1226–1236. https://doi.org/10.2307/2641210.

Arnell, N.W., 1996. Global Warming, River Flows and WaterResources. Wiley, Chichester, United Kingdom.

Argenti, G., Chiesi, M., Fibbi, L., Maselli, F., 2022. Use of remote sensing and biogeochemical models to estimate the net carbon fluxes of managed mountain grasslands. Ecol. Model. 474, 110152. https://doi.org/10.1016/j.ecolmodel.2022.110152.

Bai, Y., Cotrufo, M.F., 2022. Grassland soil carbon sequestration: current understanding, challenges, and solutions. Science (1979) 377, 603–608. https://doi.org/10.1126/science.abo2380.

Baldocchi, D., Falge, E., Gu, L., Olson, R., Hollinger, D., Running, S., Anthoni, P., Bernhofer, C., Davis, K., Evans, R., Fuentes, J., Goldstein, A., Katul, G., Law, B., Lee, X., Malhi, Y., Meyers, T., Munger, W., Oechel, W., Paw, K.T., Pilegaard, K., Schmid, H.P., Valentini, R., Verma, S., Vesala, T., Wilson, K., Wofsy, S., 2001. FLUXNET: A new tool to study the temporal and spatial variability of ecosystem-scale carbon dioxide, water vapor, and energy flux densities. B. Am. Meteorol. Soc 82, 2415–2434. https://doi.org/10.1175/1520-0477(2001)0822.3.

Barneze, A.S., Abdalla, M., Whitaker, J., McNamara, N.P., Ostle, N.J., 2022. Predicted soil greenhouse gas emissions from climate × management interactions in temperate grassland. Agronomy 12, 3055. https://doi.org/10.3390/agronomy12123055.

Bellini, E., Moriondo, M., Dibari, C., Leolini, L., Staglianò, N., Stendardi, L., Filippa, G., Galvagno, M., Argenti, G., 2022. Impacts of climate change on European grassland phenology: A 20-year analysis of MODIS satellite data. Remote Sens 15 (1), 218. https://doi.org/10.3390/rs15010218.

Bellini, E., Martin, R., Argenti, G., Staglianò, N., Costafreda-Aumedes, S., Dibari, C., Moriondo, M., Bellocchi, G., 2023a. Opportunities for adaptation to climate change of extensively grazed pastures in the Central Apennines (Italy). Land. (Basel) 12, 351. https://doi.org/10.3390/land12020351.

Bellini, E., Moriondo, M., Dibari, C., Bindi, M., Staglianò, N., Cremonese, E., Filippa, G., Galvagno, M., Argenti, G., 2023b. VISTOCK: A simplified model for simulating grassland systems. Eur. J. Agron. 142, 126647. https://doi.org/10.1016/j.eja.2022.126647.

Berry, J., Bjorkman, O., 1980. Photosynthetic response and adaptation to temperature in higher plants. Ann. Rev. Plant Physio. 31, 491–543. https://doi.org/10.1146/annurev.pp.31.060180.002423.

Bindi, M., Bellesi, S., Orlandini, S., Fibbi, L., Moriondo, M., Sinclair, T., 2005. Influence of water deficit stress on leaf area development and transpiration of Sangiovese grapevines grown in pots. Am. J. Enol. Viticult. 56, 68–72. https://doi.org/10.5344/ajev.2005.56.1.68.

Brilli, L., Bechini, L., Bindi, M., Carozzi, M., Cavalli, D., Conant, R., Dorich, C.D., Doro, L., Ehrhardt, F., Farina, R., Ferrise, R., Fitton, N., Francaviglia, R., Grace, P., Iocola, I., Klumpp, K., Léonard, J., Martin, R., Massad, R.S., Recous, S., Seddaiu, G., Sharp, J., Smith, P., Smith, W.N., Soussana, J.F., Bellocchi, G., 2017. Review and analysis of strengths and weaknesses of agro-ecosystem models for simulating C and N fluxes. Sci. Total. Environ. 598, 445–470. https://doi.org/10.1016/j.scitotenv.2017.03.208.

Brilli, L., Lugato, E., Moriondo, M., Gioli, B., Toscano, P., Zaldei, A., Leolini, L., Cantini, C., Caruso, G., Gucci, R., Merante, P., Dibari, C., Ferrise, R., Bindi, M., Costafreda-Aumedes, S., 2019. Carbon sequestration capacity and productivity responses of Mediterranean olive groves under future climates and management options. Mitig. Adapt. Strat. Gl. 24, 467–491. https://doi.org/10.1007/s11027-018-9824-x.

Brilli, L., Martin, R., Argenti, G., Bassignana, M., Bindi, M., Bonet, R., Choler, P., Cremonese, E., Della Vedova, M., Dibari, C., Filippa, G., Galvagno, M., Leolini, L., Moriondo, M., Piccot, A., Stendardi, L., Targetti, S., Bellocchi, G., 2023. Uncertainties in the adaptation of alpine pastures to climate change based on remote sensing products and modelling. J. Environ. Manag. 336, 117575. https://doi.org/10.1016/j.jenvman.2023.117575.

Bristow, K.L., Campbell, G.S., 1984. On the relationship between incoming solar radiation and daily maximum and minimum temperature. Agr. Forest Meteorol. 31, 159–166. https://doi.org/10.1016/0168-1923(84)90017-0.

Bojanowski, J.S., 2016. sirad: functions for calculating daily solar radiation and evapotranspiration. R. Package Version 2, 3-3.

Bolinder, M.A., Kätterer, T., Andrén, O., Parent, L.E., 2012. Estimating carbon inputs to soil in forage-based crop rotations and modeling the effects on soil carbon dynamics in a Swedish long-term field experiment. Can. J. Soil Sci. 92, 821–833. https://doi.org/10.4141/cjss2012-036.

Buis, S., Lecharpentier, P., Vezy, R., Giner, M., 2020. SticsRpacks: a set of packages for managing Stics from R. In XIIth Stics users seminar (p. 13).

Chabbi, A., Rumpel, C., Klumpp, K., Franzluebbers, A.J., 2023. Managing grasslands to optimize soil carbon sequestration. In Understanding and Fostering Soil Carbon Sequestration; Rumpel, C., Ed.; Burleigh Dodds Science Publishing: Cambridge, UK; ISBN 978-1-78676-969-5.

Chang, J., Ciais, P., Gasser, T., Smith, P., Herrero, M., Havlík, P., Obesteiner, M., Guenet, B., Goll, D.S., Li, W., Naipal, V., Peng, S., Qiu, VC., Tian, H., Viovy, N., Yue, C., Zhu, D., 2021a. Climate warming from managed grasslands cancels the

cooling effect of carbon sinks in sparsely grazed and natural grasslands. Nat. Commun. 12, 1–10. https://doi.org/10.1038/s41467-020-20406-7.
Chang, Q., Xiao, X., Doughty, R., Wu, X., Jiao, W., Qin, Y., 2021b. Assessing variability of optimum air temperature for photosynthesis across site-years, sites and biomes and their effects on photosynthesis estimation. Agric. Forest Meteorol. 298, 108277. https://doi.org/10.1016/j.agrformet.2020.108277.
Cherif, S., Doblas-Miranda, E., Lionello, P., Borrego, C., Giorgi, F., Iglesias, A., Jebari, S., Mahmoudi, E., Moriondo, M., Pringault, O., Rilov, G., Somot, S., Tsikliras, A., Vila, M., Zittis, G., 2020. Drivers of change. In: climate and environmental change in the Mediterranean Basin – Current situation and risks for the future. First Mediterranean Assessment Report [Cramer W, Guiot J, Marini K (eds.)] Union For the Mediterranean, Plan Bleu, UNEP/MAP, Marseille, France, 59–180.
Christie, E.K., 2014. NPP Grassland: Charleville, Australia, 1973-1974. Oak Ridge National Laboratory Distributed Active Archive Center, Oak Ridge, Tennessee, USA. 10.3334/ORNLDAAC/468. R1. Data set. Available on-line, http://daac.ornl.gov.
Coleman, K., Jenkinson, D.S., 1996. RothC-26.3-A model for the turnover of carbon in soil. In Evaluation of Soil Organic Matter models: Using Existing Long-Term Datasets. Springer Berlin Heidelberg. pp. 237–246.
Collalti, A., Tjoelker, M.G., Hoch, G., Mäkelä, A., Guidolotti, G., Heskel, M., Petit, G., Ryan, M.G., Battipaglia, G., Prentice, I.C., 2020. Plant respiration: controlled by photosynthesis or biomass? Glob. Change Biol. 26, 1739–1753. https://doi.org/10.1111/gcb.14857.
Conant, R.T., Cerri, C.E., Osborne, B.B., Paustian, K., 2017. Grassland management impacts on soil carbon stocks: a new synthesis. Ecol. Appl. 27, 662–668. https://doi.org/10.1002/eap.1473.
Dal Prà, A., Davolio, R., Immovilli, A., Burato, A., Ronga, D., 2023. Plant composition and feed value of first cut permanent meadows. Agronomy 13, 681. https://doi.org/10.3390/agronomy13030681.
De Bruijn, A.M.G., Calanca, P., Ammann, C., Fuhrer, J., 2012. Differential long-term effects of climate change and management on stocks and distribution of soil organic carbon in productive grasslands. Biogeosciences. 9, 1997–2012. https://doi.org/10.5194/bg-9-1997-2012.
Del Grosso, S.J., Parton, W.J., Adler, P.R., Davis, S.C., Keough, C., Marx, E., 2012. DayCent model simulations for estimating soil carbon dynamics and greenhouse gas fluxes from agricultural production systems. In: [Eds: Liebig, M.A., Franzluebbers, A. J., Follett, R.F] Managing Agricultural Greenhouse Gases. Academic Press. New York, NY: Elsevier Inc. 241–250. http://dx.doi.org/10.1016/b978-0-12-386897-8.00014-0.
Dibari, C., Pulina, A., Argenti, G., Aglietti, C., Bindi, M., Moriondo, M., Mula, L., Pasqui, M., Seddaiu, G., Roggero, P.P., 2021. Climate change impacts on the Alpine, Continental and Mediterranean grassland systems of Italy: A review. Ital. J. Agron. 16. https://doi.org/10.4081/ija.2021.1843.
Doughty, R., Xiao, X., Wu, X., Zhang, Y., Bajgain, R., Zhou, Y., Qin, Y., Zou, Z., McCarthy, H., Friedman, J., Wagle, P., Basara, J., Steiner, J., 2018. Responses of gross primary production of grasslands and croplands under drought, pluvial, and irrigation conditions during 2010–2016, Oklahoma, USA. Agr. Water Manage. 204, 47–59. https://doi.org/10.1016/j.agwat.2018.04.001.
FAO, 2019. FAOSTAT – Land cover statistics. Food and Agriculture Organization of the United Nations. URL: https://www.fao.org/3/cb8133en/cb8133en.pdf (accessed 24/07/2023).
Feigenwinter, I., Hörtnagl, L., Zeeman, M.J., Eugster, W., Fuchs, K., Merbold, L., Buchmann, N., 2023. Large inter-annual variation in carbon sink strength of a permanent grassland over 16 years: impacts of management practices and climate. Agr. Forest Meteorol. 340, 109613. https://doi.org/10.1016/j.agrformet.2023.109613.
Filippa, G., Cremonese, E., Galvagno, M., Migliavacca, M., Morra di Cella, U., Petey, M., Siniscalco, C., 2015. Five years of phenological monitoring in a mountain grassland: inter-annual patterns and evaluation of the sampling protocol. Int. J. Biometeorol. 59, 1927–1937. https://doi.org/10.1007/s00484-015-0999-5.
Forster, D., Deng, J., Harrison, M.T., Shurpali, N., 2022. Simulating soil-plant-climate interactions and greenhouse gas exchange in boreal grasslands using the DNDC model. Land. (Basel) 11, 1947. https://doi.org/10.3390/land11111947.
Franks, P.J., Adams, M.A., Amthor, J.S., Barbour, M.M., Berry, J.A., Ellsworth, D.S., Farquhar, G.D., Ghannoum, O., Lloyd, J., McDowell, N., Norby, R.J., Tissue, D.T., Von Caemmerer, S., 2013. Sensitivity of plants to changing atmospheric CO2 concentration: from the geological past to the next century. New. Phytol. 197, 1077–1094. https://doi.org/10.1111/nph.12104.
Garcia-Moya, E., 2015. NPP Grassland: Montecillo, Mexico, 1984–1994. Oak Ridge National Laboratory Distributed Active Archive Center, Oak Ridge, Tennessee, USA. R1. Data set. Available on-line, http://daac.ornl.gov. 10.3334/ORNLDAAC/413.
Garcia-Pausas, J., Casals, P., Romanyà, J., Vallecillo, S., Sebastià, M.T., 2011. Seasonal patterns of belowground biomass and productivity in mountain grasslands in the Pyrenees. Plant Soil. 340, 315–326. https://doi.org/10.1007/s11104-010-0601-1.
Gilmanov, T.G., 2015. NPP Grassland: Shortandy, Kazakhstan, 1977-1980. Oak Ridge National Laboratory Distributed Active Archive Center, Oak Ridge, Tennessee, USA. R1. Data set. Available on-line http://daac.ornl.gov. 10.3334/ORNLDAAC/153.
Gurung, R.B., Ogle, S.M., Breidt, F.J., Williams, S.A., Parton, W.J., 2020. Bayesian calibration of the DayCent ecosystem model to simulate soil organic carbon dynamics and reduce model uncertainty. Geoderma 376, 114529. https://doi.org/10.1016/j.geoderma.2020.114529.
Habermann, E., Dias de Oliveira, E.A., Contin, D.R., Delvecchio, G., Viciedo, D.O., de Moraes, M.A., de Mello Prado, R., de Pinho Costa, K.A., Braga, M.R., Martinez, C.A., 2019. Warming and water deficit impact leaf photosynthesis and decrease forage quality and digestibility of a C4 tropical grass. Physiol. Plantarum 165, 383–402. https://doi.org/10.1111/ppl.12891.
Hargreaves, G.H., Samani, Z.A., 1982. Estimating potential evapotranspiration. J. Irr. Drain. Div-ASCE 108, 225–230. https://doi.org/10.1061/JRCEA4.0001390.
He, L., Mostovoy, G., 2019. Cotton yield estimate using Sentinel-2 data and an ecosystem model over the southern US. Remote Sens 11. https://doi.org/10.3390/rs11172000, 2000.
Heinsch, F.A., Reeves, M., Votava, P., Kang, S., Milesi, C., Zhao, M., Glassy, J., Jolly, W. M., Loehman, R., Bowker, C.F., Kimball, J.S., Nemani, R.R., Running, S.W., 2003. User's guide GPP and NPP (MOD17A2/A3) products NASA MODIS land algorithm. Version 2.0, December 2, 2003.
Hikosaka, K., Ishikawa, K., Borjigidai, A., Muller, O., Onoda, Y., 2006. Temperature acclimation of photosynthesis: mechanisms involved in the changes in temperature dependence of photosynthetic rate. J. Exp. Bot. 57, 291–302. https://doi.org/10.1093/jxb/erj049.
IPCC, 2013. Annex II: climate system scenario tables. In: Stocker, T.F., Qin, D., Plattner, G.-K., Tignor, M., Allen, S.K., Boschung, J. et al. (eds.). Climate Change 2013: The Physical Science Basis. Contribution of Working Group I to the Fifth Assessment Report of the Intergovernmental Panel On Climate Change. Cambridge University Press, Cambridge, United Kingdom and New York, NY, USA.
IPCC, 2014. Climate Change 2014: Synthesis Report. Contribution of Working Groups I, II and III to the Fifth Assessment Report of the Intergovernmental Panel on Climate Change [Core Writing Team, R.K. Pachauri and L.A. Meyer (eds.)]. IPCC, Geneva, Switzerland, 151 pp.
Jenkinson, D.S., Harkness, D.D., Vance, E.D., Adams, D.E., Harrison, A.F., 1992. Calculating net primary production and annual input of organic matter to soil from the amount and radiocarbon content of soil organic matter. Soil. Biol. Biochem. 24, 295–308. https://doi.org/10.1016/0038-0717(92)90189-5.
Jenkinson, D.S., Hart, P.B.S., Rayner, J.H., Parry, L.C., 1987. Modelling the turnover of organic matter in long-term experiments at Rothamsted. INTECOL Bullet. 15, 1–8.
Kaonga, M.L., Coleman, K., 2008. Modelling soil organic carbon turnover in improved fallows in eastern Zambia using the RothC-26.3 model. Forest Ecol. Manag. 256, 1160–1166. https://doi.org/10.1016/j.foreco.2008.06.017.
Karatassiou, M., Noitsakis, B., 2010. Changes of the photosynthetic behaviour in annual C 3 species at late successional stage under environmental drought conditions. Photosynthetica 48, 377–382. https://doi.org/10.1007/s11099-010-0049-9.
Kellner, J., Multsch, S., Houska, T., Kraft, P., Müller, C., Breuer, L., 2017. A coupled hydrological-plant growth model for simulating the effect of elevated CO2 on a temperate grassland. Agr. Forest Meteorol. 246, 42–50. https://doi.org/10.1016/j.agrformet.2017.05.017.
Khalil, M.I., Fornara, D.A., Osborne, B., 2020. Simulation and validation of long-term changes in soil organic carbon under permanent grassland using the DNDC model. Geoderma 361, 114014. https://doi.org/10.1016/j.geoderma.2019.114014.
Köppen, W.P., 1936. Das Geographische System der Klimate: Mit 14 Textfiguren. Borntraeger, Berlin.
Lasslop, G., Reichstein, M., Papale, D., Richardson, A.D., Arneth, A., Barr, A., Stoy, P., Wohlfahrt, G., 2010. Separation of net ecosystem exchange into assimilation and respiration using a light response curve approach: critical issues and global evaluation. Glob. Change Biol. 16, 187–208. https://doi.org/10.1111/j.1365-2486.2009.02041.x.
Laub, M., Necpalova, M., Van de Broek, M., Corbeels, M., Ndungu, S.M., Mucheru-Muna, M.W., Mugendi, D., Yegon, R., Waswa, W., Vanlauwe, B., Six, J., 2023. A robust DayCent model calibration to assess the potential impact of integrated soil fertility management on maize yields, soil carbon stocks and greenhouse gas emissions in Kenya. EGUsphere 1–47. https://doi.org/10.5194/egusphere-2023-1738.
Li, C., Frolking, S., Frolking, T.A., 1992a. A model of nitrous oxide evolution from soil driven by rainfall events: I. Model structure and sensitivity. J. Geophys. Res. 97, 9759–9776. https://doi.org/10.1029/92JD00509.
Li, C., Frolking, S., Frolking, T.A., 1992b. A model of nitrous oxide evolution from soil driven by rainfall events: II. Model applications. J. Geophys. Res. 97, 9777–9783. https://doi.org/10.1029/92JD00510.
Marconi, S., Chiti, T., Nolè, A., Valentini, R., Collalti, A., 2017. The role of respiration in estimation of net carbon cycle: coupling soil carbon dynamics and canopy turnover in a novel version of 3D-CMCC forest ecosystem model. Forests. 8, 220. https://doi.org/10.3390/f8060220.
Maselli, F., Argenti, G., Chiesi, M., Angeli, L., Papale, D., 2013. Simulation of grassland productivity by the combination of ground and satellite data. Agr. Ecosyst. Environ. 165, 163–172. https://doi.org/10.1016/j.agee.2012.11.006.
Mastalerczuk, G., Borawska-Jarmułowicz, B., 2021. Physiological and morphometric response of forage grass species and their biomass distribution depending on the term and frequency of water deficiency. Agronomy 11, 2471. https://doi.org/10.3390/agronomy11122471.
Mayel, S., Jarrah, M., Kuka, K., 2021. How does grassland management affect physical and biochemical properties of temperate grassland soils? A review study. Grass. Forage Sci. 76, 215–244. https://doi.org/10.1111/gfs.12512.
Morais, T.G., Teixeira, R.F., Domingos, T., 2019. Detailed global modelling of soil organic carbon in cropland, grassland and forest soils. PLoS. One 14, e0222604. https://doi.org/10.1371/journal.pone.0222604.
Moriondo, M., Leolini, L., Brilli, L., Dibari, C., Tognetti, R., Giovannelli, A., Rapi, B., Battista, P., Caruso, G., Gucci, R., Argenti, G., Raschi, A., Centritto, M., Cantini, C., Bindi, M., 2019. A simple model simulating development and growth of an olive grove. Eur. J. Agron. 105, 129–145. https://doi.org/10.1016/j.eja.2019.02.002.
Moss, R.H., Edmonds, J.A., Hibbard, K.A., Manning, M.R., Rose, S.K., van Vuuren, D.P., Carter, T.R., Emori, S., Kainuma, M., Kram, T., Meehl, G.A., Mitchell, J.F.B., Nakicenovic, N., Riahi, K., Smith, S.J., Stouffer, R.J., Thomson, A.M., Weyant, J.P., Wilbanks, T.J., 2010. The next generation of scenarios for climate change research and assessment. Nature 463, 747–756. https://doi.org/10.1038/nature08823.

Movedi, E., Bellocchi, G., Argenti, G., Paleari, L., Vesely, F., Staglianò, N., Dibari, C., Confalonieri, R., 2019. Development of generic crop models for simulation of multi-species plant communities in mown grasslands. Ecol. Modell. 401, 111–128. https://doi.org/10.1016/j.ecolmodel.2019.03.001.

Movedi, E., Paleari, L., Argenti, G., Vesely, F.M., Staglianò, N., Parrini, S., Confalonieri, R., 2024. The application of a plant community model to evaluate adaptation strategies for alleviating climate change impacts on grassland productivity, biodiversity and forage quality. Ecol. Modell. 488, 110596. https://doi.org/10.1016/j.ecolmodel.2023.110596.

Necpálová, M., Anex, R.P., Fienen, M.N., Del Grosso, S.J., Castellano, M.J., Sawyer, J.E., Iqbal, J., Pantoja, J.L., Barker, D.W., 2015. Understanding the DayCent model: calibration, sensitivity, and identifiability through inverse modeling. Environ. Modell. Softw. 66, 110–130. https://doi.org/10.1016/j.envsoft.2014.12.011.

Noce, S., Collalti, A., Valentini, R., Santini, M., 2016. Hot spot maps of forest presence in the Mediterranean basin. IForest. 9, 766–774. https://doi.org/10.3832/ifor1802-009.

Parton, W.J., Hartman, M., Ojima, D., Schimel, D., 1998. DAYCENT and its land surface submodel: description and testing. Global Planet. Change 19, 35–48. https://doi.org/10.1016/S0921-8181(98)00040-X.

Parton, W.J., Ojima, D.S., Cole, C.V., Schimel, D.S., 1994. A general model for soil organic matter dynamics: sensitivity to litter chemistry, texture and management. Quant. Model. Soil Form. Process. 39, 147–167. https://doi.org/10.2136/sssaspecpub39.c9.

Pastorello, G., Trotta, C., Canfora, E., Chu, H., Christianson, D., Cheah, Y.W., Papale, D., 2020. The FLUXNET2015 dataset and the ONEFlux processing pipeline for eddy covariance data. Sci. Data 7, 1–27. https://doi.org/10.1038/s41597-020-0534-3.

Petersen, K., Kraus, D., Calanca, P., Semenov, M.A., Butterbach-Bahl, K., Kiese, R., 2021. Dynamic simulation of management events for assessing impacts of climate change on pre-alpine grassland productivity. Eur. J. Agron. 128, 126306. https://doi.org/10.1016/j.eja.2021.126306.

Pintaldi, E., D'Amico, M.E., Siniscalco, C., Cremonese, E., Celi, L., Filippa, G., Prati, M., Freppaz, M., 2016. Hummocks affect soil properties and soil-vegetation relationships in a subalpine grassland (North-Western Italian Alps). Catena (Amst) 145, 214–226. https://doi.org/10.1016/j.catena.2016.06.014.

Poggio, L., De Sousa, L.M., Batjes, N.H., Heuvelink, G., Kempen, B., Ribeiro, E., Rossiter, D., 2021. SoilGrids 2.0: producing soil information for the globe with quantified spatial uncertainty. Soil 7, 217–240. https://doi.org/10.5194/soil-7-217-2021.

Porter, H., Jong, R., 1999. A comparison of specific leaf area, chemical composition and leaf construction costs of field plants from 15 habitats differing in productivity. New. Phytol. 143, 163–176. https://doi.org/10.1046/j.1469-8137.1999.00428.x.

Pulina, A., Lai, R., Salis, L., Seddaiu, G., Roggero, P.P., Bellocchi, G., 2018. Modelling pasture production and soil temperature, water and carbon fluxes in Mediterranean grassland systems with the Pasture Simulation model. Grass and Forage Sci. 73 (2), 272–283. https://doi.org/10.1111/gfs.12310.

Rafique, R., Kumar, S., Luo, Y., Kiely, G., Asrar, G., 2015. An algorithmic calibration approach to identify globally optimal parameters for constraining the DayCent model. Ecol. Modell. 297, 196–200. https://doi.org/10.1016/j.ecolmodel.2014.11.022.

Reich, P.B., Walters, M.B., Ellsworth, D.S., Vose, J.M., Volin, J.C., Gresham, C., Bowman, W.D., 1998. Relationships of leaf dark respiration to leaf nitrogen, specific leaf area and leaf life-span: a test across biomes and functional groups. Oecologia 114, 471–482. https://doi.org/10.1007/s004420050471.

Reichstein, M., Falge, E., Baldocchi, D., Papale, D., Aubinet, M., Berbigier, P., Bernhofer, C., Buchmann, N., Gilmanov, T., Granier, A., Grünwald, T., Havránková, K., Ilvesniemi, H., Janous, D., Knohl, A., Laurila, T., Lohila, A., Loustau, D., Matteucci, G., Meyers, T., Miglietta, F., Ourcival, J.M., Pumpanen, J., Rambal, S., Rotenberg, E., Sanz, M., Tenhunen, J., Seufert, G., Vaccari, F., Vesala, T., Yakir, D., Valentini, R., 2005. On the separation of net ecosystem ex-change into assimilation and ecosystem respiration: review and improved algorithm. Glob. Change Biol. 11, 1424–1439. https://doi.org/10.1111/j.1365-2486.2005.001002.x.

Riedo, M., Grub, A., Rosset, M., Fuhrer, J., 1998. A pasture simulation model for dry matter production, and fluxes of carbon, nitrogen, water and energy. Ecol. Model. 105, 141–183. https://doi.org/10.1016/S0304-3800(97)00110-5.

Rouse, J.W., Haas, R.H., Schell, J.A., Deering, D.W., 1974. Monitoring Vegetation Systems in the Great Plains With ERTS. NASA Spec. Publ, 351, 309.

Roy, J., Picon-Cochard, C., Augusti, A., Benot, M.L., Thiery, L., Darsonville, O., Landais, D., Piel, C., Defossez, M., Devidal, S., Escape, C., Ravel, O., Fromin, N., Volaire, F., Milcu, A., Bahn, M., Soussana, J.F., 2016. Elevated CO2 maintains grassland net carbon uptake under a future heat and drought extreme. P. Natl. Acad. Sci. 113, 6224–6229. https://doi.org/10.1073/pnas.1524527113.

Running, S.W., Zhao, M., 2019. Daily GPP and annual NPP (MOD17A2H/A3H) and year-end gap-filled (MOD17A2HGF/A3HGF) products NASA Earth Observing System MODIS land algorithm. MOD17.

Ryan, E.M., Ogle, K., Peltier, D., Walker, A.P., De Kauwe, M.G., Medlyn, B.E, Williams, D. G., Parton, W., Asao, S., Guenet, B., Harper, A.B., Lu, X., Luus, K.A., Zaehle, S., Shu, S., Werner, C., Xia, J., Pendall, E., 2017. Gross primary production responses to warming, elevated CO2, and irrigation: quantifying the drivers of ecosystem physiology in a semiarid grassland. Glob. Change Biol. 23, 3092–3106. https://doi.org/10.1111/gcb.13602.

Sándor, R., Barcza, Z., Acutis, M., Doro, L., Hidy, D., Köchy, M., Minet, J., Lellei-Kovacs, E., Ma, S., Perego, A., Rolinski, S., Ruget, F., Sanna, M., Seddaiu, G., Wu, L., Bellocchi, G., 2017. Multi-model simulation of soil temperature, soil water content and biomass in Euro-Mediterranean grasslands: uncertainties and ensemble performance. Eur. J. Agron. 88, 22–40. https://doi.org/10.1016/j.eja.2016.06.006.

Sándor, R., Ehrhardt, F., Grace, P., Recous, S., Smith, P., Snow, V., Soussana, J.F., Basso, B., Bhatiai, A., Brilli, L., Doltra, J., Dorich, C.D., Doro, L., Fitton, N., Grant, B., Harrison, M.T., Kirschbaum, M.U.F., Klumpp, K., Laville, P., Léonard, J., Martin, R., Massad, R.S., Moore, A., Myrgiotis, V., Pattey, E., Rolinski, S., Sharp, J., Skiba, U., Smith, W., Wu, L., Zhang, Q., Bellocchi, G., 2020. Ensemble modelling of carbon fluxes in grasslands and croplands. Field Crop. Res. 252, 107791. https://doi.org/10.1016/j.fcr.2020.107791.

Schleip, I., Lattanzi, F.A., Schnyder, H., 2013. Common leaf life span of co-dominant species in a continuously grazed temperate pasture. Basic Appl. Ecol. 14, 54–63. https://doi.org/10.1016/j.baae.2012.11.004.

Seeber, J., Tasser, E., Rubatscher, D., Loacker, I., Lavorel, S., Robson, T.M., Balzarolo, M., Altimir, N., Drösler, M., Vescovo, L., Gamper, S., Barančok, P., Staszewski, T., Wohlfahrt, G., Cernusca, A., Sebastia, M.T., Tappeiner, U., Bahn, M., 2022. Effects of land use and climate on carbon and nitrogen pool partitioning in European mountain grasslands. Sci. Total. Environ. 822, 153380. https://doi.org/10.1016/j.scitotenv.2022.153380.

Sierra, C.A., Müller, M., Trumbore, S.E., 2012. Models of soil organic matter decomposition: the SoilR package, version 1.0. Geosci. Model Dev 5, 1045–1060. https://doi.org/10.5194/gmd-5-1045-2012.

Sinclair, T.R., 1986. Water and nitrogen limitations in soybean grain production I. Model development. F. Crop. Res. 15, 125–141. https://doi.org/10.1016/0378-4290(86)90082-1.

Sinclair, T.R., 2006. A reminder of the limitations in using Beer's Law to estimate daily radiation interception by vegetation. Crop. Sci. 46, 2343–2347. https://doi.org/10.2135/cropsci2006.01.0044.

Soltani, A., Sinclair, T.R., 2012. Modeling Physiology of Crop development, Growth and Yield. Wallingford, Oxfordshire, UK.

Soussana, J.F., Maire, V., Gross, N., Bachelet, B., Pagès, L., Martin, R., Hill, D., Wirth, C., 2012. Gemini: A grassland model simulating the role of plant traits for community dynamics and ecosystem functioning. Parameterization and evaluation. Ecol. Modell. 231, 134–145. https://doi.org/10.1016/j.ecolmodel.2012.02.002.

Szaniawski, R.K., Kielkiewicz, M., 1982. Maintenance and growth respiration in shoots and roots of sunflower plants grown at different root temperatures. Physiol. plantarum 54, 500–504. https://doi.org/10.1111/j.1399-3054.1982.tb00716.x.

Tanner, C.B., Sinclair, T.R., 1983. Efficient water use in crop production: research or re-search? In: Taylor, H.M., Jordan, W.R. and Sinclair, T.R. (eds) Limitations to Efficient Water Use in Crop Production. American Society of Agronomy, Crop Science Society of America, and Soil Science Society of America, Madison, Wisconsin, pp. 1–27.

Thornley, J.H.M., Cannell, M.G.R., 2000. Modelling the components of plant respiration: representation and realism. Ann. Bot-London 85, 55–67. https://doi.org/10.1006/anbo.1999.0997.

Trnka, M., Kocmánková, E., Balek, J., Eitzinger, J., Ruget, F., Formayer, H., Hlavinka, P., Schaumberger, A., Horáková, V., Mozny, M., Žalud, Z., 2010. Simple snow cover model for agrometeorological applications. Agr. Forest Meteorol. 150, 1115–1127. https://doi.org/10.1016/j.agrformet.2010.04.012.

Veroustraete, F., Sabbe, H., Rasse, D.P., Bertels, L., 2004. Carbon mass fluxes of forests in Belgium determined with low resolution optical sensors. Int. J. Remote Sens. 25, 769–792. https://doi.org/10.1080/0143116031000115238.

Wallach, D., Buis, S., Lecharpentier, P., Bourges, J., Clastre, P., Launay, M., Bergez, J.E., Guerif, M., Soudais, J., Justes, E., 2011. A package of parameter estimation methods and implementation for the STICS crop-soil model. Environ. Model. Softw. 26, 386–394. https://doi.org/10.1016/j.envsoft.2010.09.004.

Wang, F., Harindintwali, J.D., Yuan, Z., Wang, M., Wang, F., Li, S., Chen, J.M., 2021. Technologies and perspectives for achieving carbon neutrality. Innovation 2.

Wang, N., Quesada, B., Xia, L., Butterbach-Bahl, K., Goodale, C.L., Kiese, R., 2019a. Effects of climate warming on carbon fluxes in grasslands—A global meta-analysis. Glob. Change Biol. 25, 1839–1851.

Wang, J., Sun, J., Yu, Z., Li, Y., Tian, D., Wang, B., Li, Z., Niu, S., 2019b. Vegetation type controls root turnover in global grasslands. Glob. Ecol. Biogeogr. 28, 442–455. https://doi.org/10.1111/geb.12866.

Whitman, W., Lauenroth, W.K., 2014. NPP Grassland: Dickinson, USA, 1970, R1. Oak Ridge National Laboratory Distributed Active Archive Center, Oak Ridge, Tennessee, USA. 10.3334/ORNLDAAC/207. Data set. Available on-line, daac.ornl.gov.

Wohlfahrt, G., Hammerle, A., Haslwanter, A., Bahn, M., Tappeiner, U., Cernusca, A., 2008. Seasonal and inter-annual variability of the net ecosystem CO2 exchange of a temperate mountain grassland: effects of weather and management. J. Geophys. Res.-Atmos. 113 (D8). https://doi.org/10.1029/2007JD009286.

Xu, X., Liu, W., Kiely, G., 2011. Modeling the change in soil organic carbon of grassland in response to climate change: effects of measured versus modelled carbon pools for

initializing the Rothamsted Carbon model. Agric. Ecosyst. Environ. 140, 372–381. https://doi.org/10.1016/j.agee.2010.12.018.

Xu, X., Sherry, R.A., Niu, S., Li, D., Luo, Y., 2013. Net primary productivity and rain-use efficiency as affected by warming, altered precipitation, and clipping in a mixed-grass prairie. Glob. Change Biol. 19, 2753–2764. https://doi.org/10.1111/gcb.12248.

Yang, Y., Dou, Y., An, S., Zhu, Z., 2018. Abiotic and biotic factors modulate plant biomass and root/shoot (R/S) ratios in grassland on the Loess Plateau. China. Sci. Total Environ. 636, 621–631. https://doi.org/10.1016/j.scitotenv.2018.04.260.

Yin, S., Zhang, X., Lyu, J., Zhi, Y., Chen, F., Wang, L., Liu, C., Zhou, S., 2020. Carbon sequestration and emissions mitigation in paddy fields based on the DNDC model: A review. Artif. Intell. Agric. 4, 140–149. https://doi.org/10.1016/j.aiia.2020.07.002.

Zani, C.F., Abdalla, M., Abbott, G.D., Taylor, J.A., Galdos, M.V., Cooper, J.M., Lopez-Capel, E., 2023. Predicting long-term effects of alternative management practices in conventional and organic agricultural systems on soil carbon stocks using the DayCent model. Agronomy 13, 1093. https://doi.org/10.3390/agronomy13041093.

Zhao, Y., Liu, Z., Wu, J., 2020. Grassland ecosystem services: a systematic review of research advances and future directions. Landsc. Ecol. 35, 793–814.

Zimmermann, M., Leifeld, J., Schmidt, M.W.I., Smith, P., Fuhrer, J., 2007. Measured soil organic matter fractions can be related to pools in the RothC model. Eur. J. Soil. Sci. 58, 658–667. https://doi.org/10.1111/j.1365-2389.2006.00855.x.